processes

MDPI

Article

Synthesis, Characterization, and Biological Evaluation of Novel *N*-{4-[(4-Bromophenyl)sulfonyl]benzoyl}-*L*-valine Derivatives

Theodora-Venera Apostol [1,*], Mariana Carmen Chifiriuc [2], Laura-Ileana Socea [1], Constantin Draghici [3], Octavian Tudorel Olaru [1,*], George Mihai Nitulescu [1], Diana-Carolina Visan [1], Luminita Gabriela Marutescu [2], Elena Mihaela Pahontu [1], Gabriel Saramet [1] and Stefania-Felicia Barbuceanu [1]

[1] Faculty of Pharmacy, "Carol Davila" University of Medicine and Pharmacy, 6 Traian Vuia Street, District 2, 020956 Bucharest, Romania
[2] Department of Botany and Microbiology, Faculty of Biology, University of Bucharest, 1-3 Intrarea Portocalelor, District 6, 60101 Bucharest, Romania
[3] "Costin D. Nenițescu" Centre of Organic Chemistry, Romanian Academy, 202 B Splaiul Independenței, District 6, 060023 Bucharest, Romania
* Correspondence: theodora.apostol@umfcd.ro (T.-V.A.); octavian.olaru@umfcd.ro (O.T.O.)

Abstract: In this article, we present the design and synthesis of novel compounds, containing in their molecules an *L*-valine residue and a 4-[(4-bromophenyl)sulfonyl]phenyl moiety, which belong to *N*-acyl-α-amino acids, 4*H*-1,3-oxazol-5-ones, 2-acylamino ketones, and 1,3-oxazoles chemotypes. The synthesized compounds were characterized through elemental analysis, MS, NMR, UV/VIS, and FTIR spectroscopic techniques, the data obtained are in accordance with the assigned structures. Their purities were verified by reversed-phase HPLC. The new compounds were tested for antimicrobial action against bacterial and fungal strains for antioxidant activity by DPPH, ABTS, and ferric reducing power assays, and for toxicity on freshwater cladoceran *Daphnia magna* Straus. Furthermore, in silico studies were performed concerning the potential antimicrobial effect and toxicity. The results of antimicrobial activity, antioxidant effect, and toxicity assays, as well as of in silico analysis revealed a promising potential of *N*-{4-[(4-bromophenyl)sulfonyl]benzoyl}-*L*-valine and 2-{4-[(4-bromophenyl)sulfonyl]phenyl}-4-isopropyl-4*H*-1,3-oxazol-5-one for developing novel antimicrobial agents to fight Gram-positive pathogens, and particularly *Enterococcus faecium* biofilm-associated infections.

Keywords: *N*-acyl-*L*-valine; 4*H*-1,3-oxazol-5-one; 2-acylamino ketone; 1,3-oxazole; diphenyl sulfone scaffold; drug design; in silico studies; antimicrobial and antibiofilm actions; antioxidant effect; alternative toxicity testing

Citation: Apostol, T.-V.; Chifiriuc, M.C.; Socea, L.-I.; Draghici, C.; Olaru, O.T.; Nitulescu, G.M.; Visan, D.-C.; Marutescu, L.G.; Pahontu, E.M.; Saramet, G.; et al. Synthesis, Characterization, and Biological Evaluation of Novel *N*-{4-[(4-Bromophenyl)sulfonyl]benzoyl}-*L*-valine Derivatives. *Processes* **2022**, *10*, 1800. https://doi.org/10.3390/pr10091800

Academic Editors: Iliyan Ivanov and Stanimir Manolov

Received: 17 August 2022
Accepted: 3 September 2022
Published: 7 September 2022

1. Introduction

Antimicrobial resistance represents a significant threat to global health and development today. Without effective antimicrobials (e.g., antibiotics, antifungals, and antiparasitics) and antiviral drugs, the success of modern medicine in preventing and treating infections would be at increased risk [1]. The discovery and development of new antimicrobial agents are therefore of considerable importance and one of the main focuses of today's scientific community is the synthesis and identification of potent active substances.

An exhaustive survey of the literature on natural and synthetic oxazole-based molecules shows that they have numerous biological properties, which include antibacterial, antifungal, anti-inflammatory, antioxidant, and cytotoxic activities [2–11]. For example, a physiologically important active cyclic peptide with a 1,3-oxazole ring is dalfopristin, a semi-synthetic streptogramin A antibiotic analog marketed under the trade name Synercid in the combination with quinupristin, a streptogramin B derivative. The structures of some representative antimicrobial agents containing the 1,3-oxazole skeleton are shown in Figure 1.

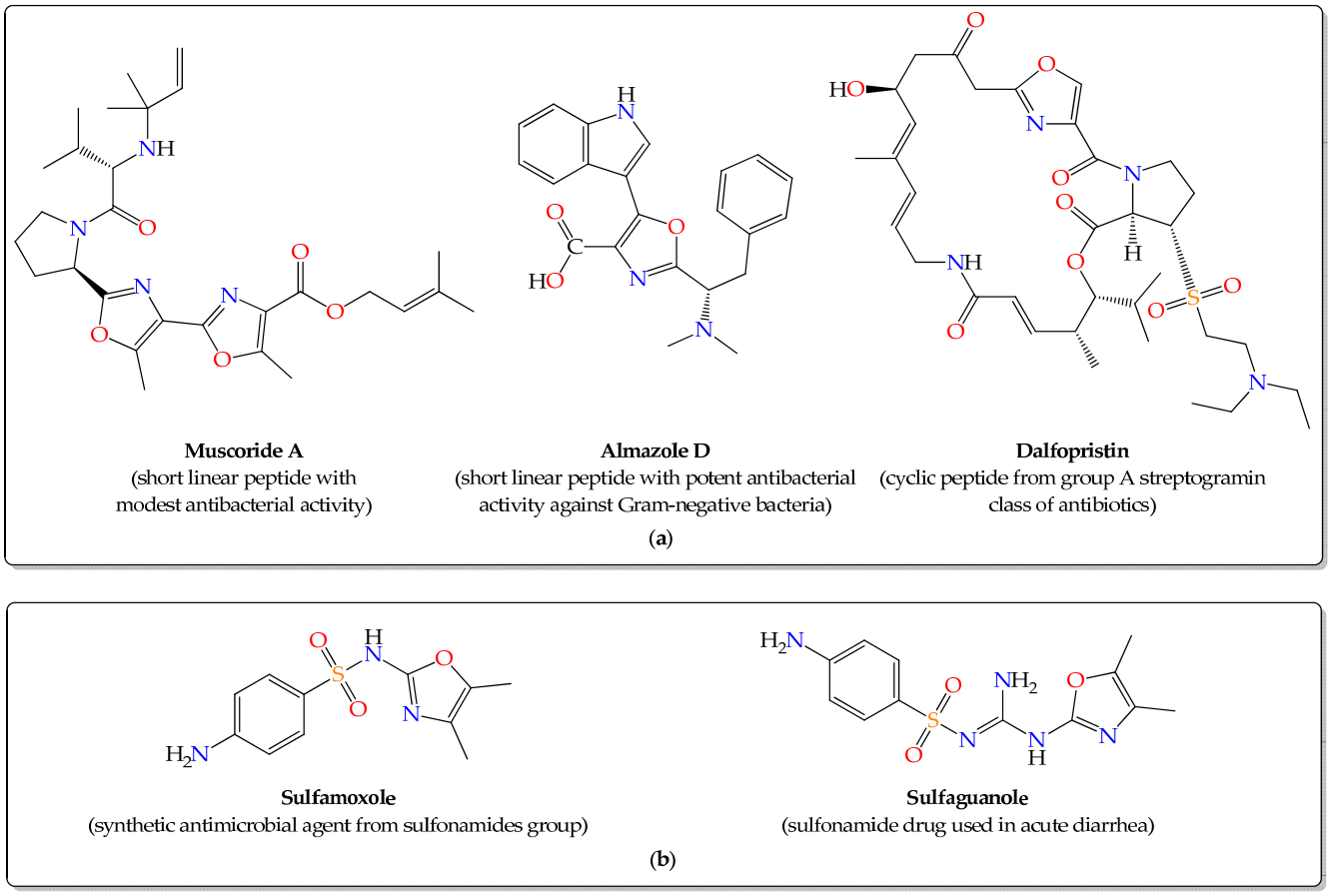

Figure 1. Structures of some representative bioactive compounds sharing the 1,3-oxazole scaffold as antimicrobial agents: (**a**) Natural or semi-synthetic products; (**b**) Synthetic compounds.

The isolable 5-keto-tautomers of 1,3-oxazol-5-ols are 5-oxo-4,5-dihydro-1,3-oxazoles, known as 4*H*-1,3-oxazol-5-ones or 2-oxazolin-5-ones, which are also mentioned for their antimicrobial, cytotoxic, antiprotozoal, and antiviral properties [12–15]. Moreover, the *N*-acylated α-amino acids are reported to display many pharmaceutical activities, such as antimicrobial, antiviral, anticancer, mucolytic, antioxidant, and antihypertensive effects [16–22], and the 2-acylamino ketones present antiviral, anti-inflammatory, antithrombotic, and antihypertensive actions [23–28].

Furthermore, diaryl sulfones represent an important class of bioactive compounds with diverse biological properties, including antimicrobial and antioxidant actions [29–37]. The structural prototype of this class is dapsone (4,4′-sulfonyldianiline, 4,4′-diaminodiphenyl sulfone, DDS), which is used alone or as part of a multi-drug regimen in the treatment or prophylaxis of certain infectious diseases, such as leprosy (also known as Hansen's disease). Currently, the therapeutic potential of organic compounds with a sulfonyl group in their molecules is being studied extensively [38,39]. In this regard, a new drug candidate from the organosulfones class is masupirdine (SUVN-502), a 1-[(2-bromophenyl)sulfonyl]-1*H*-indole derivative with a selective 5-HT_6 receptor antagonist effect, developed for the symptomatic treatment of Alzheimer's disease [40].

Based on the promising therapeutic potential of these scaffolds and in the continuation of our research [41–46], we designed, obtained, and characterized novel *L*-valine-derived analogs with a 4-[(4-bromophenyl)sulfonyl]phenyl fragment and also evaluated their in silico and in vitro antimicrobial, antioxidant, and toxicity properties with the aim of identifying new biologically active compounds. The used synthesis methodology enables synthetic chemical diversification with the potential to prepare drug-like compounds.

The in silico approach to the biological activity of the new bromine compounds allowed the assessment of their toxicity and potential antimicrobial effect.

The in vitro antimicrobial testing of the new compounds included both qualitative screening (measuring the diameters of the zones of inhibition of microbial growth) and quantitative analysis (determining the values of minimal inhibitory concentration), as well as the assay of the antibiofilm action (determining the values of minimal biofilm inhibitory concentration). Particular emphasis was placed on evaluating the inhibition of microbial adhesion to surfaces as a possible means of reducing the burden of biofilm-associated infections.

The in vitro antioxidant activity of newly obtained compounds was investigated colorimetrically according to three electron transfer-based methods, namely 2,2-diphenyl-1-picrylhydrazyl (DPPH) assay, 2,2′-azino-bis(3-ethylbenzothiazoline-6-sulfonic acid) (ABTS) radical cation test, and ferric reducing power assay.

The compounds' toxicity was assessed on *Daphnia magna*. This bioassay is a widely used method for the toxicity evaluation of natural and synthetic compounds, and it is in accordance with the "3 R's" (reduction, refinement, and replacement) concept regarding experiments on vertebrates. It can be used as a prescreening method for rats and other mammals' acute toxicity tests. The main advantage of this method is the crustacean reproduction mode by parthenogenesis, which leads to populations with lower variability than other invertebrate species [47,48].

2. Results

2.1. Drug Design Strategy

2.1.1. Structure-Based Similarity Analysis

Based on our previous research on *N*-{4-[(4-chlorophenyl)sulfonyl]benzoyl}-*L*-valine derivatives as antimicrobial and antibiofilm agents, we made modifications in the structures of the target molecules by replacing the chlorine atom with the more lipophilic bromine atom. The objective of this study was to increase the lipophilic character of the newly synthesized compounds while maintaining the substituent's electronic effects. The proposed structures **5**–**8** were virtually explored on the ChEMBL database to demonstrate their original character and to assess their antimicrobial potential using similar compounds.

The search for similar compounds of *N*-acyl-*L*-valine **5** and α-acylamino ketones **7a** and **7b** returned 34 results and no similar structure for 4*H*-1,3-oxazol-5-one **6** and 1,3-oxazoles **8a** and **8b**, highlighting the originality of the proposed structures. No antimicrobial results were found for the 34 structurally similar compounds recorded in ChEMBL.

The substructure search based on the common 1-bromo-4-(phenylsulfonyl)benzene scaffold returned 32 compounds with 237 registered minimal inhibitory concentration (MIC) values, ranging from 2.5 up to 1024 μg/mL. All 32 compounds share an R-{4-[(4-bromophenyl)sulfonyl]phenyl} structure (Figure 2). The wide range of the MIC values indicates that the nature of the R group is very important for the potency of the antimicrobial effect. The lipophilic character of the compounds, expressed by the clogP value, seems to confirm the hypothesis of a better antimicrobial effect for most tested bacterial strains (Figure 2). The newly designed bromo derivatives have clogP values above the average of their similar compounds, indicating a potentially improved antimicrobial effect.

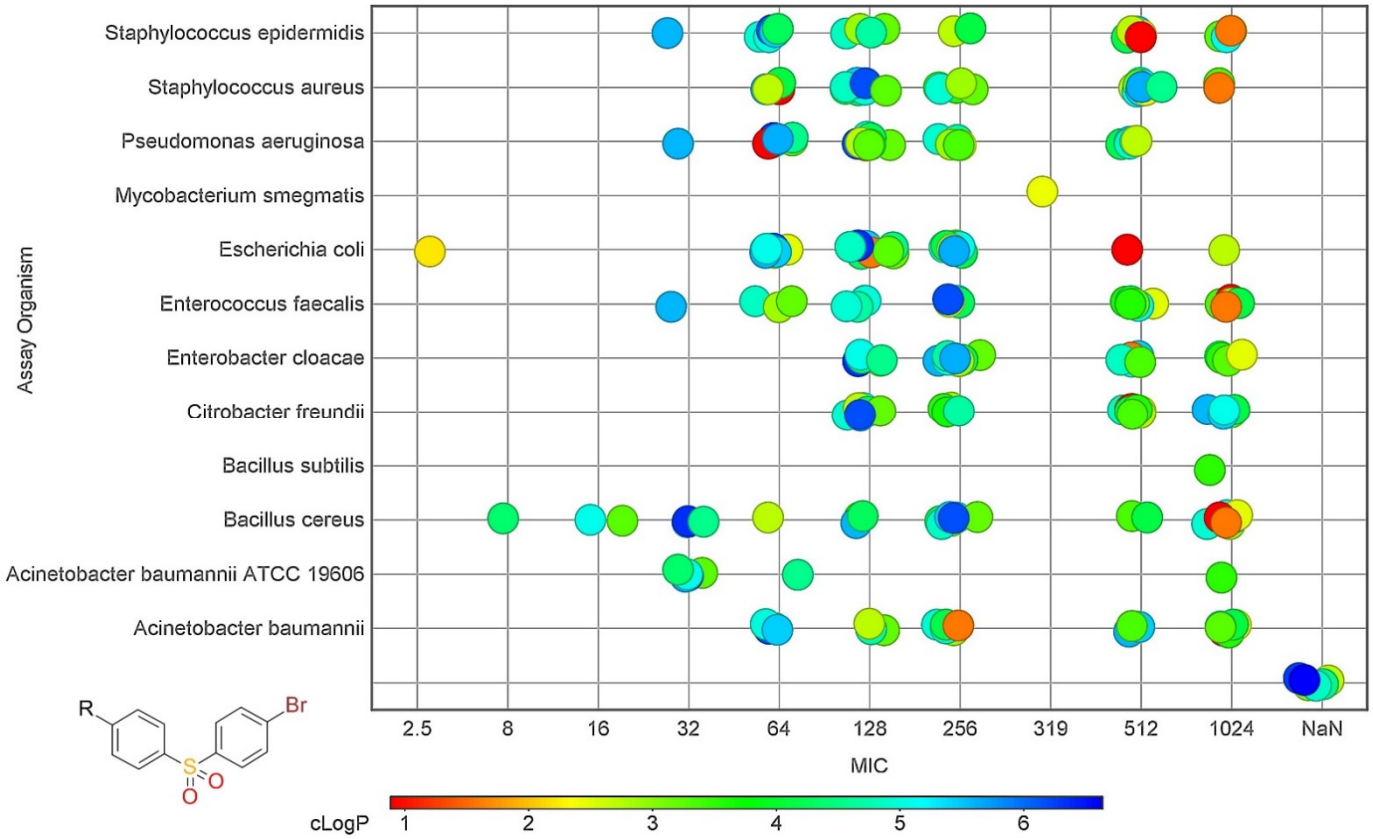

Figure 2. MIC values for the compounds resulted after the substructure search based on the 1-bromo-4-(phenylsulfonyl)benzene scaffold. NaN presents the new compounds **5**, **6**, **7a**,**b**, and **8a**,**b**.

2.1.2. PASS Prediction

The 2D chemical structure of each target compound was input into the PASS application to obtain the probability of the corresponding compound to produce (Pa) or not (Pi) a certain biological effect. The application returns an array of Pa and Pi values for a very wide variety of pharmacological actions [49]. In the case of newly synthesized compounds **5**, **6**, **7a**, **7b**, **8a**, and **8b**, the 896 listed biological activities were filtered in relation to the antibacterial effect. The predicted probabilities Pa and Pi are presented in Table 1.

Table 1. PASS predicted the probabilities that the new compounds **5**, **6**, **7a**,**b**, and **8a**,**b** to be active (Pa) as antimicrobial agents.

Target	5	6	7a	7b	8a	8b
Antibiotic glycopeptide-like	-	0.40	-	-	-	-
Antimycobacterial	0.49	0.58	0.51	0.51	0.36	0.37
Antituberculosis	0.48	0.41	0.49	0.49	0.30	0.30
Anti-infective	0.58	0.37	0.36	0.41	0.30	0.34

The two new α-acylamino ketones **7a** and **7b** were predicted to have very similar chances to produce antimycobacterial, antituberculosis, or anti-infective effects, and the corresponding values are significantly higher than those of the 1,3-oxazoles derivatives **8a** and **8b**. The Pa values reflect the likelihood of a certain effect to be produced, and not of its potency. Based on the Pa values, the addition of an aromatic fragment to *N*-acylated *L*-valine **5** has little impact on its predicted antimycobacterial and antituberculosis activities.

2.2. Chemistry

2.2.1. Synthesis of the New Compounds

The synthesis of new 4-[(4-bromophenyl)sulfonyl]benzoic acid derivatives **5**–**8** was performed according to the synthetic route, as outlined in Scheme 1.

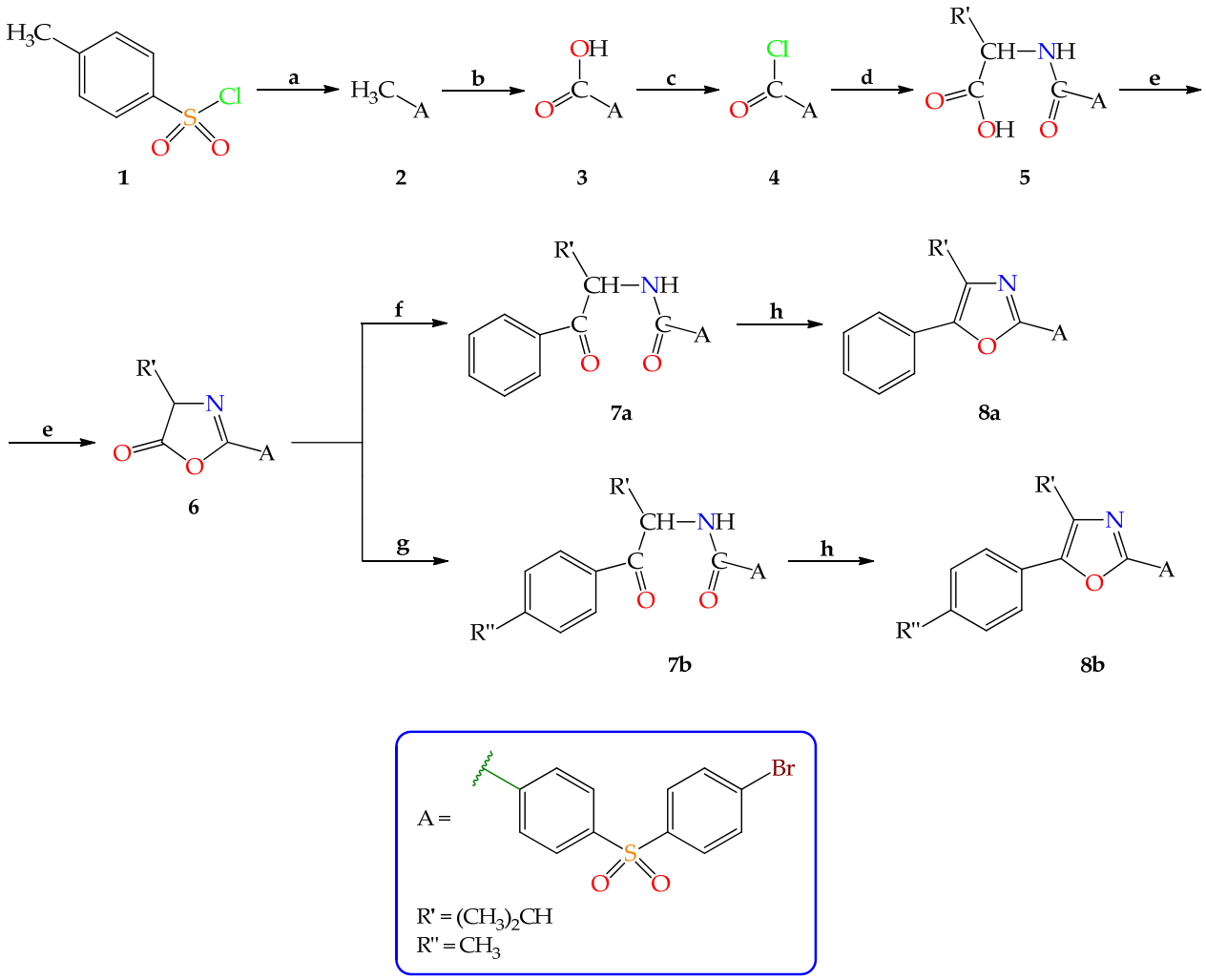

Scheme 1. Synthesis pathway for the obtainment of new *N*-{4-[(4-bromophenyl)sulfonyl]benzoyl}-*L*-valine analogs. Reagents and reaction conditions: (**a**) $C_6H_5Br/AlCl_3$, reflux; (**b**) CrO_3/CH_3COOH, reflux [50]; (**c**) $SOCl_2$, reflux, 30 h, 99% yield [46]; (**d**) (i) *L*-valine/NaOH, CH_2Cl_2, 0–5 °C, 30 min; (ii) rt (room temperature), 1 h; (iii) 2 N hydrochloric acid; 94% yield; (**e**) ethyl chloroformate/4-methylmorfoline, CH_2Cl_2, rt, 30 min, 90% yield; (**f**) $C_6H_6/AlCl_3$, rt, 20 h, 80% yield; (**g**) $C_6H_5CH_3/AlCl_3$, rt, 20 h, 86% yield; (**h**) $POCl_3$, reflux, 4 h, 91% (**8b**) and 94% (**8a**) yields.

The key starting material, 4-[(4-bromophenyl)sulfonyl]benzoic acid **3** was prepared by Friedel–Crafts sulfonylation of bromobenzene with commercially available tosyl chloride **1** in presence of aluminum trichloride, followed by oxidation of the sulfonation product (1-bromo-4-tosylbenzene) **2** with chromium trioxide in acetic acid [50]. The previously obtained compound **3** was then transformed by reaction with chlorinating reagent $SOCl_2$ to the corresponding acyl chloride **4** [46,51], which was used in the next step in the raw state. Subsequently, the 2-{4-[(4-bromophenyl)sulfonyl]benzamido}-3-methylbutanoic acid **5** was synthesized via Schotten–Baumann-type *N*-acylation of *L*-valine with 4-[(4-bromophenyl)sulfonyl]benzoyl chloride **4** in dichloromethane at room temperature with a reaction yield of 94%. The 2-{4-[(4-bromophenyl)sulfonyl]phenyl}-4-isopropyl-4*H*-1,3-oxazol-5-one **6** was produced by intramolecular cyclodehydration of compound **5** in presence of ethyl chloroformate and 4-methylmorpholine at room temperature in 90% yield.

Then, the *N*-(1-aryl-3-methyl-1-oxobutan-2-yl)-4-[(4-bromophenyl)sulfonyl]benzamides **7a**,**b** were obtained via Friedel–Crafts acylation of aromatic hydrocarbons (benzene, toluene) with 2-oxazolin-5-one **6** using anhydrous $AlCl_3$ as catalyst at room temperature in about 83% yield. Finally, the 5-aryl-2-{4-[(4-bromophenyl)sulfonyl]phenyl}-4-isopropyl-1,3-oxazoles **8a**,**b** were prepared via Robinson–Gabriel-type intramolecular cyclization reaction of the 2-acylamino ketones **7a**,**b** with phosphoryl trichloride at reflux in yields of 91% (**8b**) and 94% (**8a**). Structure elucidation of all newly synthesized *L*-valine derivatives was performed by means of spectral (UV/VIS, FTIR, NMR, MS) and elemental analyses.

2.2.2. Spectroscopic Characterization of the New Compounds

Various spectral analysis methods were applied to perform the detailed structural characterization of the newly obtained 4-[(4-bromophenyl)sulfonyl]benzoic acid derivatives **5**–**8**, the resulting data being consistent with the depicted molecular structures.

Ultraviolet and Visible Absorption Spectroscopy Data

The UV/VIS absorption spectra of novel compounds **5**–**8** dissolved in methanol presented bands at 202.6 nm (**5**–**8**), at 227.3 nm (**6**), in the 249.3–255.5 nm region (**5**–**8**), and at 333.9 (**8a**) or 337.4 nm (**8b**). When acetonitrile was used as solvent, the first peak was shifted in the interval of 195.3–198.0 nm (**5**–**8**), while the rest of the bands were recorded at approximately the same wavelength values: at 228.2 nm (for **5**, this peak appearing as a "shoulder" when methanol was used as solvent) or 229.1 nm (**6**), in the range of 248.6–254.8 nm (**5**–**8**), and at 335.6 (**8a**) or 340.1 nm (**8b**). The last absorption maximum was present only in the electronic spectra of compounds **8a** and **8b** due to the extension of the π-electron conjugation by the formation of the 1,3-oxazole chromophore.

Fourier-Transform Infrared Absorption Spectroscopy Data

The FTIR absorption spectra of acyclic precursors **5** and **7** showed a characteristic peak in the range of 3347–3281 cm^{-1} due to the valence vibration of the N–H bond. In addition, the absorption maximum at 1746 cm^{-1} due to carbonyl valence vibration, and another at 1635 cm^{-1} due to stretching vibration of amidic carbonyl were remarked in the FTIR spectrum of **5**. For α-acylamino ketones **7a** and **7b**, these two carbonyl absorption bands are overlapped, as suggested by the very strong single peak recorded in their FTIR spectra at 1655 cm^{-1}. A broad absorption band in the spectral region from 3300 to 2500 cm^{-1}, centered at $\approx$ 3000 cm^{-1}, due to stretching vibration of the O–H bond and two noticeably weak satellite peaks at 2676 and 2599 cm^{-1} are also characteristic of the hydrogen-bonded *N*-acylated *L*-valine **5**.

As evidence that the intramolecular cyclocondensations occurred, significant changes were observed in the FTIR absorption spectra of five-membered *O*,*N*-heterocyclic compounds **6**, and **8a**,**b** compared with the corresponding spectra of open-chain intermediates **5**, and **7a**,**b**, respectively. The FTIR spectrum of 4*H*-1,3-oxazol-5-one **6** presented a peak at 1825 cm^{-1} due to carbonyl stretching vibration, which is shifted at a higher wavenumber compared with the C=O absorption maximum from the spectrum of **5**. The FTIR absorption spectra of 5-membered heterocycles **6** and **8** showed an absorption band at 1650 (**6**), 1602 (**8a**), or 1601 cm^{-1} (**8b**) due to the valence vibration of the C=N bond. The absorption maxima at 1099 (**8a**), 1097 (**8b**), or 1040 cm^{-1} (**6**) due to the C–O–C symmetric stretching vibration and at 1280 (**8a** and **8b**) or 1243 cm^{-1} (**6**) due to the asymmetric stretching vibration of the C–O–C group were also observed.

Nuclear Magnetic Resonance Spectroscopy Data

The nuclear magnetic resonance spectroscopic data also confirmed the structures of the new *L*-valine analogs. Complete assignments of the signals from the ^{1}H and ^{13}C NMR spectra of the new compounds **5**–**8** were performed using combinations of standard NMR spectroscopic techniques, namely 2D COSY and HETCOR experiments.

The molecular structures of the new bromine-containing derivatives **5**–**8** with the numbering of the atoms, used for the assignment of NMR signals, are presented in Figure 3.

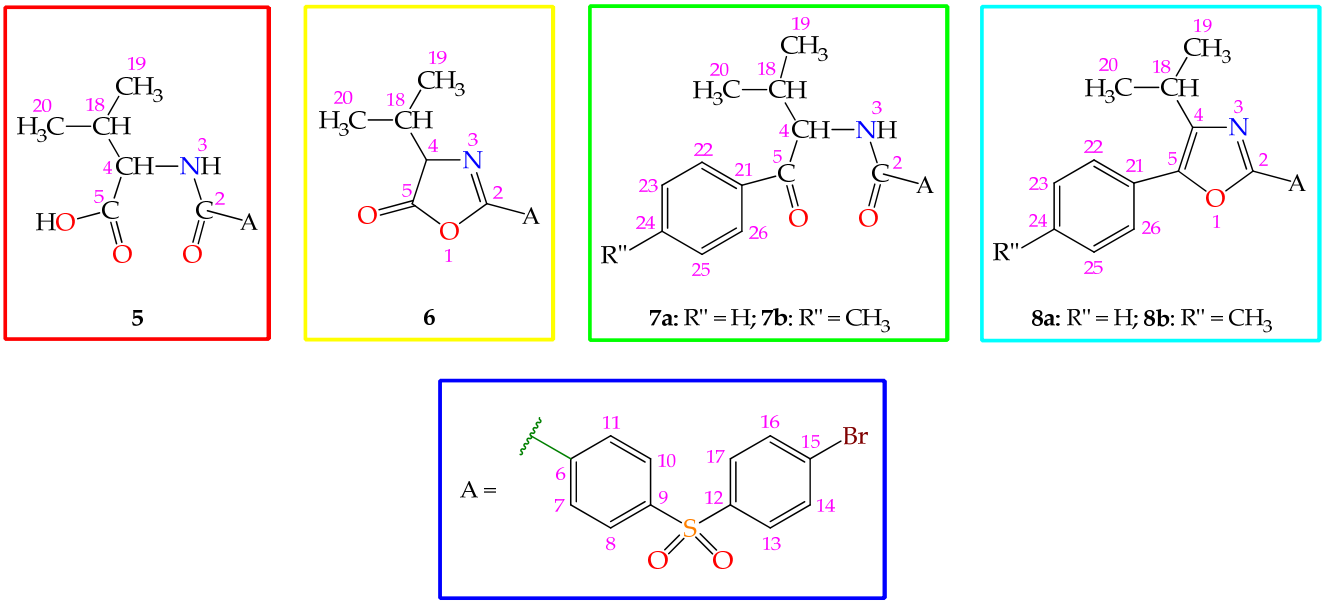

Figure 3. Molecular structures of the new 4-[(4-bromophenyl)sulfonyl]benzoic acid derivatives **5**–**8** with the atom numbering (for assigning NMR signals).

Proton NMR Spectroscopy Data

The proton NMR spectra of **5** and **7** showed a doublet signal in the region between 8.73 and 8.99 ppm, attributed to deshielded H-3 proton. The ^{1}H NMR spectrum of **5** revealed a signal assigned to the H-4 proton at 4.29 ppm as a doublet of doublets due to the vicinal coupling to H-3 and H-18 protons. The proton NMR spectra of α-acylamino ketones **7a** and **7b** showed the H-4 signal at 5.36 (**7b**) or 5.38 ppm (**7a**) as a triplet, due to the coupling to H-3 and H-18. The ^{1}H NMR spectra of **5**, **7a**, and **7b** also highlighted characteristic signals for the isopropyl substituent, i.e., an octet (**5**) or a multiplet (**7a**,**b**) signal registered in the range of 2.17–2.28 ppm assigned to the methine proton (H-18) and two strongly shielded doublet signals, the first in the interval of 0.89–0.94 ppm and the second at 0.92 or 0.95 ppm, due to the non-equivalent protons (H-19, H-20) of the two methyl groups. The signal of proton of the carboxyl group of *N*-acyl-α-amino acid **5** was not recorded in the ^{1}H NMR spectrum probably due to hydrogen-deuterium exchange, but the presence of the COOH group was confirmed both by IR and ^{13}C NMR spectral data.

The ^{1}H NMR spectrum of **6** displayed the H-4 doublet signal at 4.32 ppm due to the coupling only to the H-18 proton (with ^{3}J = 4.7 Hz). The methine proton of the 1-methylethyl group was revealed by the presence of a septet of doublets signal at 2.40 ppm due to coupling to protons H-19, H-20 (with ^{3}J = 6.9 Hz), and to H-4 proton (with ^{3}J = 4.7 Hz). The ^{1}H NMR spectra of **8a** and **8b** showed for the isopropyl substituent a signal as septet at 3.26 (**8b**) or 3.29 ppm (**8a**) attributed to the H-18 proton, and a shielded doublet at 1.35 (**8b**) or 1.36 ppm (**8a**), due to the two CH_3 groups' protons.

Carbon-13 NMR Spectroscopy Data

The ^{13}C NMR spectrum of *N*-acylated *L*-valine **5** presented a signal at 58.43 ppm attributed to the C-4, for the 1-methylethyl group revealed a signal at 29.48 ppm due to the methine carbon (C-18) and two signals at 18.61 and 19.25 ppm due to the C-19 and C-20 non-equivalent carbon atoms. The ^{13}C NMR spectrum of **6** highlighted the C-4 signal at 71.04 ppm, which is deshielded by 12.61 ppm as a result of cyclization of the open-chain precursor **5**. Further, the C-2 atom of 4*H*-1,3-oxazol-5-one **6** resonated at 160.36 ppm, being

more shielded with 5.42 ppm compared with the C-2 of **5**, and the C-5 at 176.98 ppm, being more deshielded with 4.19 ppm than the corresponding carbon atom of its precursor (**5**).

The carbon-13 NMR spectra of aromatic *O*,*N*-heterocycles **8a**,**b** showed a signal assigned to the C-4 atom at 143.63 (**8b**) or 144.19 ppm (**8a**), which is more deshielded by ≈ 84.77 ppm than the corresponding signal of the compounds from which they were obtained by cyclization, from 59.05 (**7b**) or 59.23 ppm (**7a**). The cyclization of **7a**,**b** to compounds **8a**,**b** induced a shielding effect for the C-2 of the 1,3-oxazole ring, resulting in an about 7.87 ppm lower chemical shift. The C-5 signal of 1,3-oxazoles **8a**,**b** was observed at 145.47 (**8a**) or 145.69 ppm (**8b**), whereas the corresponding signal of acyclic precursors **7a**,**b** appeared at 198.57 (**7b**) or 199.19 ppm (**7a**), revealing a shift of this carbon signal at a smaller δ_C of approximately 53.30 ppm.

Gas Chromatography Coupled to Electron Ionization Mass Spectrometry Data

For saturated azlactone **6**, supplementary evidence was obtained by its mass spectrum obtained by GC/EI–MS analysis. The two molecular ions of compound **6** corresponding to bromine isotopes (^{79}Br/^{81}Br) were energetically unstable upon interaction with high-energy (70 eV) electrons and fragmented with the elimination of a molecule of propene. The base peak with m/z 381 and the corresponding cation-radical with m/z 379 (with a relative abundance of 71.61%) were resulted according to the ^{79}Br/^{81}Br isotopic ratio of ≈1:1. Other characteristic structural fragments of **6** are reported in the Materials and Methods section.

2.3. Evaluation of Antimicrobial Activity

2.3.1. Qualitative Assessment of Antimicrobial Activity

The agar diffusion assay showed that compounds **7a**, **8a**, and **8b** did not interfere with microbial growth (Table 2). *Enterococcus faecium* E5 was the most susceptible species to compounds **5** and **6** with a growth inhibition zone diameter of 17 and 15 mm, respectively. Compounds **6** and **7b** also inhibited the growth of *Staphylococcus aureus* ATCC 6538 and *Bacillus subtilis* ATCC 6683, respectively with diameters of growth inhibition zones of 8 mm and of 10 mm.

Table 2. Results of the qualitative analysis of the antimicrobial effect of compounds **5**–**8** tested at 5000 µg/mL, using an adapted disk diffusion method (diameters of growth inhibition zones were measured in mm).

Tested Compound	Gram-Positive Bacteria			Gram-Negative Bacteria		Fungus
	Bacillus subtilis ATCC 6683	*Enterococcus faecium* E5	*Staphylococcus aureus* ATCC 6538	*Escherichia coli* ATCC 8739	*Pseudomonas aeruginosa* ATCC 27857	*Candida albicans* 393
5	0	17	0	0	0	0
6	0	15	8	0	0	0
7a	0	0	0	0	0	0
7b	10	0	0	0	0	0
8a	0	0	0	0	0	0
8b	0	0	0	0	0	0
Ciprofloxacin	28	30	26	34	30	-*
Fluconazole	-	-	-	-	-	30

* -: not tested.

2.3.2. Effects of Compounds on Antibiotic Susceptibility Profile

For compounds **5** and **6** only, their influence on the *E. faecium* E5 and *S. aureus* ATCC 6538 strains' susceptibility to different antibiotics was evaluated. Although compound **7b** was active against *B. subtilis* ATCC 6683, the influence on this strain's susceptibility to antibiotics was not investigated, as there are no specific guidelines regarding the susceptibility breakpoints of this species.

No significant changes were noticed in the *E. faecium* E5 strain's susceptibility to current antibiotics after culture in the presence of compound **5** tested at subinhibitory concentration (Table 3), suggesting both a low selective pressure for resistance occurrence and a different mechanism of action. Regarding the *E. faecium* E5 strain cultured in the presence of compound **6**, it was observed that it determined an increase in the antimicrobial

effect of the tested antibiotics (ampicillin, penicillin, linezolid, and vancomycin). The diameters of growth inhibition zones (in mm) are shown in Table 3.

Table 3. Antibiotic susceptibility testing of *E. faecium* E5 strain cultured in the presence of compounds **5** and **6** tested at a subinhibitory concentration of 250 μg/mL and of dimethyl sulfoxide (DMSO) (growth inhibition zone diameters were measured in mm).

Microbial Culture	Growth Inhibition Zone Diameter (In mm)			
	Ampicillin	Linezolid	Penicillin	Vancomycin
Control *	24	27	14	19
5	22	25	13	17
6	29	39	15	23
DMSO	22	23	0	18

* liquid culture medium inoculated with standardized suspension of *E. faecium* E5.

With respect to the *S. aureus* ATCC 6538 strain cultured in the presence of compound **6**, a slight increase in the diameter of growth inhibition zone was observed in the case of cefoxitin (Table 4). Regarding other studied antibiotics, namely vancomycin, linezolid, clindamycin, and rifampicin, the susceptibility was reduced, suggesting a phenotypic change in the tested strain exposed to compound **6** at subinhibitory concentration. There were no changes in the growth inhibition zone diameters compared with those of the microbial growth control in the case of the studied antibiotics: azithromycin, penicillin, and trimethoprim-sulfamethoxazole.

Table 4. Antibiotic susceptibility testing of *S. aureus* ATCC 6538 strain cultured in the presence of compound **6** tested at 250 μg/mL and of DMSO control (growth inhibition zone diameters were measured in mm).

Microbial Culture	Growth Inhibition Zone Diameter (In mm)							
	Azithromycin	Cefoxitin	Clindamycin	Linezolid	Penicillin	Rifampicin	Trimethoprim-Sulfamethoxazole	Vancomycin
Control *	15	20	26	32	0	21	0	23
6	15	21	23	29	0	19	0	21
DMSO	13	15	20	28	0	19	0	18

* liquid culture medium inoculated with standardized suspension of *S. aureus* ATCC 6538.

2.3.3. Quantitative Testing of Antimicrobial Activity

The results of the quantitative antimicrobial testing by the standard broth microdilution method are presented in Table 5. The majority of the tested compounds exhibited MIC values equal to or higher than 500 μg/mL. The most active proved to be compound **6** which was found to have a moderate antimicrobial activity (MIC value of 250 μg/mL) against the *S. aureus* ATCC 6538 reference strain.

Table 5. MIC (minimal inhibitory concentration) and MBIC (minimal biofilm inhibitory concentration) values in μg/mL determined for compounds **5–8** tested at concentrations between 500 and 0.97 μg/mL.

Tested Compound	Gram-Positive Bacteria						Gram-Negative Bacteria				Fungus	
	Bacillus subtilis ATCC 6683		*Enterococcus faecium* E5		*Staphylococcus aureus* ATCC 6538		*Escherichia coli* ATCC 8739		*Pseudomonas aeruginosa* ATCC 27857		*Candida albicans* 393	
	MIC	MBIC	MIC	MBIC	MIC	MBIC	MIC	MBIC	MIC	MBIC	MIC	MBIC
5	>500	>500	500	62.5	>500	>500	>500	>500	>500	>500	>500	>500
6	>500	>500	500	1.95	250	250	>500	>500	>500	>500	>500	>500
7a	>500	>500	>500	>500	>500	>500	>500	>500	>500	>500	>500	>500
7b	>500	>500	>500	>500	>500	>500	>500	>500	>500	>500	>500	>500
8a	>500	>500	>500	>500	>500	>500	>500	>500	>500	>500	>500	>500
8b	>500	>500	>500	>500	>500	>500	>500	>500	>500	>500	>500	>500
Ciprofloxacin	<0.03	<0.03	0.62	0.62	0.15	0.15	0.012	0.012	0.15	0.15	- *	-
Fluconazole	-	-	-	-	-	-	-	-	-	-	<0.12	<0.12

* -, not tested.

2.3.4. Evaluation of Antibiofilm Activity

The results obtained in this study showed that compounds **7a**, **7b**, **8a**, and **8b** did not interfere with microbial adherence on surfaces. Exceptional antibiofilm activity was observed for compounds **5** and **6** against *E. faecium* E5 strain, with MBIC values of 62.5 and 1.95 μg/mL, respectively (Table 5). Compound **6** also displayed a moderate antibiofilm effect in the case of the Gram-positive *S. aureus* ATCC 6538 strain, with an MBIC value of 250 μg/mL.

2.4. Evaluation of Antioxidant Activity

The antioxidant effect of newly synthesized derivatives **5**–**8** was studied using three methods based on electron transfer reactions, namely DPPH, ABTS, and ferric reducing power tests. The results were compared with those of the following standard antioxidant agents: ascorbic acid (AA), butylated hydroxyanisole (BHA, a mixture of 2-(*tert*-butyl)-4-methoxyphenol and 3-(*tert*-butyl)-4-methoxyphenol) and butylated hydroxytoluene (BHT, 2,6-di-*tert*-butyl-4-methylphenol), used as positive controls. The antioxidant capacity of the key starting materials *L*-valine and 4-[(4-bromophenyl)sulfonyl]benzoic acid **3** was also determined.

2.4.1. Antioxidant Activity Assay by DPPH Method

The results of the study concerning the antioxidant effect evaluation of the new 4-[(4-bromophenyl)sulfonyl]benzoic acid derivatives **5**–**8** by the DPPH method are presented in Table 6. In terms of experimental results obtained by this test, of all the newly synthesized compounds, 4*H*-1,3-oxazol-5-one **6** had the best antioxidant activity with a DPPH inhibition rate of 16.75 ± 1.18%, its effect being better than that of key starting materials (*L*-valine and carboxylic acid **3**), but lower than the standard antioxidants used. This compound was followed by *N*-acylated α-amino acid **5** with a DPPH inhibition percentage of 4.70 ± 1.88%. In contrast, compounds **7a**,**b**, and **8a**,**b** had the lowest scavenging effect values in the range of 1.35–1.82%.

Table 6. Results of the assessment of the antioxidant effect of the compounds tested by the DPPH method.

Compound	Concentration (μM)	Scavenging Effect (%)
5	250	4.70 ± 1.88
6	250	16.75 ± 1.18
7a	250	1.42 ± 0.06
7b	250	1.35 ± 1.72
8a	250	1.82 ± 0.36
8b	250	1.50 ± 0.11
L-Valine	250	7.87 ± 0.07
3	250	2.32 ± 0.22
AA	250	85.09 ± 1.67
BHA	250	77.99 ± 0.56
BHT	250	31.79 ± 1.52

2.4.2. Antioxidant Activity Assay by ABTS Method

The results of the assessment of the antioxidant potential of the compounds tested by the ABTS method are shown in Table 7. The obtained values of the percentage scavenging effect of new compounds **5**–**8** are small in the interval of 0.40–7.66%. Among the new compounds, 1,3-oxazole **8b** showed the best antioxidant activity (7.66 ± 0.71%), followed by α-acylamino ketone **7a** (7.14 ± 1.51%), while compound **7b** had the lowest (0.40 ± 0.27%). By this method, *L*-valine had a better effect (44.71 ± 0.66%) than the new products **5**–**8**, but key raw material **3** showed a lower activity (0.17 ± 0.85%) than these.

Table 7. Results of the evaluation of the scavenging effect of the compounds analyzed by the ABTS method.

Compound	Concentration (μM)	Scavenging Effect (%)
5	250	0.78 ± 0.91
6	250	1.49 ± 0.37
7a	250	7.14 ± 1.51
7b	250	0.40 ± 0.27
8a	250	1.77 ± 0.56
8b	250	7.66 ± 0.71
L-Valine	250	44.71 ± 0.66
3	250	0.17 ± 0.85
AA	250	99.93 ± 0.11
BHA	250	99.74 ± 0.08
BHT	250	98.46 ± 1.23

2.4.3. Ferric Reducing Power Assay

The results of the investigation of the antioxidant capacity of the compounds tested by the ferric reducing power method are presented in Table 8. All the tested compounds possessed the ability to reduce iron(III) to iron(II). The α-acylamino ketone **7a** was a better iron(III) reducer (absorbance at 700 nm, A_{700} of 0.0722 ± 0.0013) than the other new derivatives, followed by three compounds, which showed similar values of the ferric reducing power, in descending order: **6** (A_{700} = 0.0461 ± 0.0088), **8b** (A_{700} = 0.0439 ± 0.0057), and **7b** (A_{700} = 0.0437 ± 0.0105). Of the compounds tested, *N*-acyl-*L*-valine **5** was the least active tested compound (A_{700} = 0.0224 ± 0.0019) and *L*-valine had the best antioxidant activity (A_{700} = 0.0854 ± 0.0051). None of the activities of the analyzed compounds were comparable to those of the AA, BHA, and BHT positive controls.

Table 8. Results of the screening of the antioxidant activity of the compounds tested by the ferric reducing power method.

Compound	Concentration (μM)	Reducing Power (Absorbance at 700 nm, A_{700})
5	500	0.0224 ± 0.0019
6	500	0.0461 ± 0.0088
7a	500	0.0722 ± 0.0013
7b	500	0.0437 ± 0.0105
8a	500	0.0369 ± 0.0060
8b	500	0.0439 ± 0.0057
L-Valine	500	0.0854 ± 0.0051
3	500	0.0568 ± 0.0078
AA	500	0.8727 ± 0.0315
BHA	500	1.1363 ± 0.0096
BHT	500	0.7282 ± 0.1686

2.5. Daphnia magna Toxicity Bioassay

The results of the *Daphnia magna* toxicity test are presented in Table 9, and the lethality curves are shown in Figure 4. At 24 h, the highest toxicity was induced by **7a** and **7b**, and the compounds **5**, **6**, **8a**, and **8b** were non-toxic on *D. magna* at the tested concentrations. At 48 h, the most toxic compound was **7a**. At the lowest concentration, its lethality was 65%; therefore, the LC_{50} being lower than 2 μg/mL, the estimated value by extrapolation is 0.21 μg/mL. The compounds **5**, **6**, **7b**, and **8a** induced medium to high toxicity, their LC_{50} values varying from 21.07 to 54.62 μg/mL. Except for **7a**, all compounds induced lower toxicity than the key starting material **3**. The compound **8b** at the highest concentration (50 μg/mL) induced a lethality of 25%, and at all other concentrations, the lethality varies from 0 to 10%. The predicted LC_{50} values were significantly lower than those obtained experimentally, except for compound **3**.

Table 9. *Daphnia magna* toxicity test results.

Tested Compound	Predicted LC_{50} [1] $_{(48\ h)}$ (μg/mL)	L % Max $_{(48\ h)}$ [2]	Determined $LC_{50\ (24\ h)}$ (μg/mL)	95% CI [3] of $LC_{50\ (24\ h)}$ (μg/mL)	Determined $LC_{50\ (48\ h)}$ (μg/mL)	95% CI of $LC_{50\ (48\ h)}$ (μg/mL)
5	0.51	60	ND [4] *	ND *	43.5	ND **
6	0.33	70	ND *	ND *	31.25	22.32 to 43.75
7a	0.11	100	42.93	38.14 to 48.31	ND ***	ND **
7b	0.11	90	58.83	46.28 to 74.78	21.07	12.92 to 34.35
8a	0.1	60	ND *	ND *	54.62	41.73 to 71.48
8b	0.04	30	ND *	ND *	ND *	ND *
L-Valine (Control 1)	1078.3	20	ND *	ND *	ND *	ND *
3 (Control 2)	11.8	100	31.11	ND **	1.144	0.13 to 9.93

[1] 50% lethal concentration; [2] maximum lethality induced at 48 h; [3] 95% confidence interval; [4] not determined because of the results obtained; * lethality ranged between 0 and 40%; ** 95% CI could not be determined due to the results; *** lethality was higher than 50% at all concentrations.

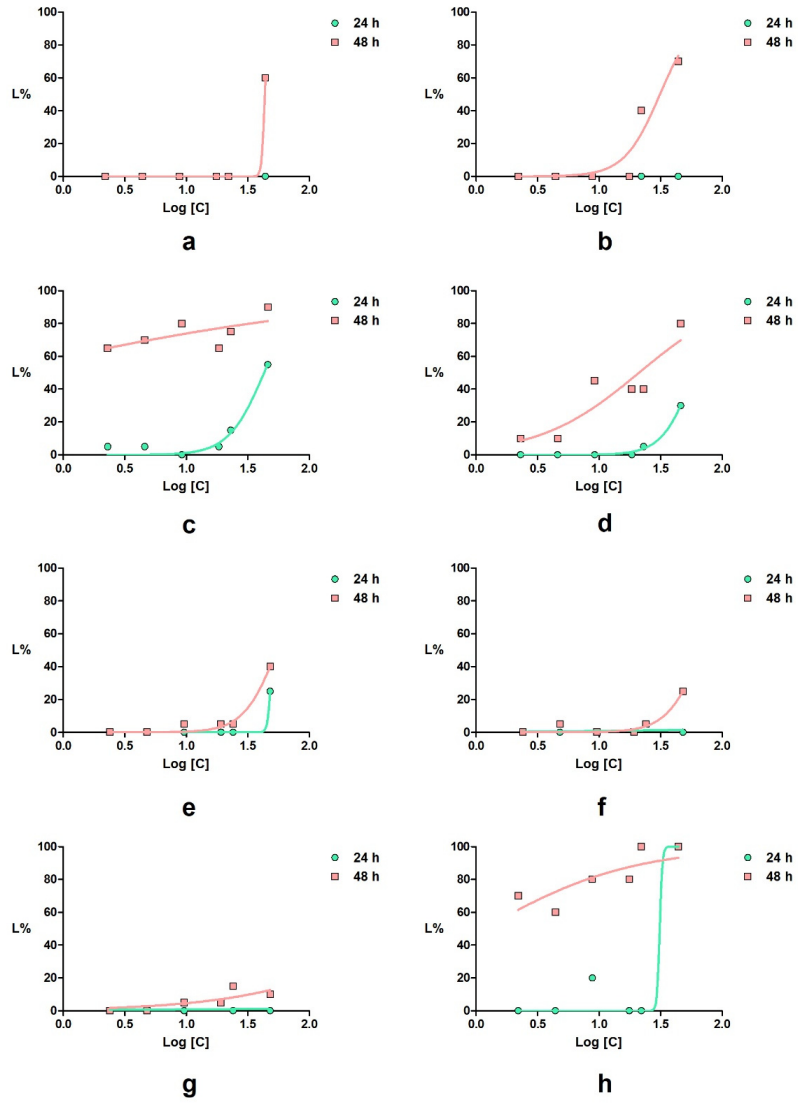

Figure 4. *Daphnia magna* lethality curves for the tested compounds: (**a**) **5**; (**b**) **6**; (**c**) **7a**; (**d**) **7b**; (**e**) **8a**; (**f**) **8b**; (**g**) *L*-valine (control 1); (**h**) **3** (control 2).

3. Discussions

The 1,3-oxazoles are five-membered heteromonocyclic scaffolds, containing two heteroatoms, O and N at positions 1 and 3, respectively, of particular importance in synthetic

and medicinal chemistry, since representatives of this class have great structural diversity and are of significant biological interest.

Over time, researchers have paid particular attention to the preparation of new derivatives incorporating the 1,3-oxazole ring [52–55], as well as to the evaluation, among other pharmacological properties, of their antimicrobial and antioxidant activities, a large number of articles being published on this topic. Currently, various bioactive 1,3-oxazole-embedded heterocycles have been reported, such as 1,3-oxazole clubbed pyridyl-pyrazolines having good to excellent antimicrobial action [56], cytisine-containing 1,3-oxazoles as potential inhibitors of *Candida* spp. glutathione reductase [57], thioxo-1,3-oxazole analogs that prevent bacterial growth and with antioxidant ability [58], 1,3-oxazole-quinoxaline amine hybrids showing antibacterial activity [59], steroidal 1,3-oxazole derivatives displaying effective antimicrobial and antibiofilm properties [60], binaphthyl-based, functionalized 1,3-oxazole peptidomimetics with moderate to excellent antimicrobial activity [61], substituted 1,3-oxazole-benzamides as antibacterial inhibitors of the essential bacterial cell division protein FtsZ [62], *N*-(oxazolylmethyl)thiazolidinediones as selective inhibitors of *Candida albicans* biofilm formation [63], and some antimicrobial 2-amino-1,3-oxazoles [64]. Very recently, we investigated the in silico and in vitro antimicrobial and antibiofilm effects of a series of 1,3-oxazole-based compounds and their isosteric analogs derived from alanine and phenylalanine, some of them presenting a promising profile [65]. Quantitative studies also indicated that of all 2,5-diaryl-1,3-oxazoles tested, only some of those with a bromine atom in their molecules showed antimicrobial and/or antibiofilm action. In contrast, all other derivatives from the same class, unsubstituted or with a chlorine atom in their structures, proved to be inactive at the concentrations tested. Other researchers have also observed that the incorporation of the chlorine or bromine atom, usually grafted onto an aromatic nucleus, led to an improvement in the antimicrobial activity of compounds of different classes, as well as that brominated derivatives have shown greater efficacy than chlorinated analogs [66–69]. The antimicrobial effect due to the presence of halogen atoms appears to be related to the compounds' relative hydrophobicity. It was found that hydrophobicity of the compounds enhanced with the addition of a halogen atom in the molecule and that chlorine derivatives displayed a less pronounced effect, while the incorporation of a bromine atom led to analogs with a higher hydrophobic profile [66]. In view of these findings, it is of interest to obtain new bromine-bearing 1,3-oxazoles-type molecules and to explore their application as biologically active agents.

In the present work, we synthesized novel organic compounds, carrying a bromine atom in their molecules, based on the 1,3-oxazole and diphenyl sulfone pharmacophores. The molecular structures of the newly obtained bromine-containing compounds (which are *N*-acyl-*L*-valine, 4-isopropyl-4*H*-1,3-oxazol-5-one, 2-acylamino ketone, and 4-isopropyl-1,3-oxazole derivatives) were elucidated based on spectroscopic investigations. Moreover, the synthesized analogs were assessed for antimicrobial properties, namely qualitative (zone of inhibition) and quantitative (MIC) activities, antibiofilm action (MBIC), and for antioxidant and toxic effects. Furthermore, in silico investigations on the toxicity and potential antimicrobial action were performed.

The structure-based similarity analysis of the new *L*-valine derivatives **5**–**8** highlighted the originality of the proposed structures and indicated that the presence of the bromine atom in the proposed structures of the new compounds can enhance the potential antimicrobial effect. The PASS prediction showed the probability that all new compounds to exhibit anti-infective, antimycobacterial, and antituberculosis activities and, in addition, that 4*H*-1,3-oxazol-5-one **6** to have a glycopeptide-like antibiotic effect.

The antimicrobial activity assays revealed a promising antimicrobial potential against Gram-positive cocci strains, particularly in the case of *E. faecium* biofilm, when the MBIC values were as from 8 to 256 times lower than the corresponding MIC values.

Concerning the results of quantitative tests for the evaluation of antimicrobial and antibiofilm activity, it was also found that the MIC and MBIC values of the standard broad-spectrum antibacterial drug ciprofloxacin and antifungal agent fluconazole, which served as

positive controls, were lower than those determined for the compounds tested. This can be explained by the fact that the novel *L*-valine derivatives, which belong to four classes, may have distinct mechanisms of action from those of the used control drugs and, in addition, unlike them, are not standardized active ingredients in optimized drug formulations.

It was also found that all compounds analyzed show antioxidant activity through all spectroscopic tests used (DPPH, ABTS, and ferric reducing power methods), but lower than the bioactive standards (AA, BHA, and BHT). The tested compounds thus demonstrated weak electron-donating properties.

The in vitro evaluation regarding antimicrobial, antioxidant, and toxicity features highlighted that acyclic intermediate **5** is promising due to its very good antibiofilm activity, low antioxidant effect, and moderate toxicity. It is worth noting that by cyclodehydration of compound **5** to the corresponding 4*H*-1,3-oxazol-5-one **6**, an increase in the antibiofilm effect and antioxidant activity was observed, but also an increase in its toxicity. Moreover, it appears that the conversion of 2-oxazolin-5-one **6** to α-acylamino ketone **7b** and the cyclization of **7b** to 1,3-oxazole **8b** leads to a decrease in antimicrobial activity, and compound **7a** and corresponding 1,3-oxazole **8a** were found to be inactive at the tested concentrations. No regular variation in the antioxidant effect of compounds **7a**, **7b**, **8a**, and **8b** was noticed, but of all the new compounds tested, **7a** and **8b** stood out, which showed the best activity by all three methods used. It was also shown that by converting saturated azlactone **6** to α-acylamino ketones **7a**,**b**, the toxicity increases, and by cyclization of open-chain intermediates **7a**,**b** to 1,3-oxazoles **8a**,**b**, the toxicity decreases significantly, **8b** being non-toxic. However, the *Daphnia magna* assay showed medium to high toxicity for compounds **5**, **6**, and **7b**, and significant-high toxicity for compounds **3** and **7a**. Our findings indicate a high potential for biological targets, whereas the 1,3-oxazole-containing compound **8b** showed no toxicity at concentrations lower than 50 μg/mL. The toxicity study also showed that, with the exception of the LC_{50} value obtained for key intermediate **3**, the experimental values of LC_{50} for all other compounds were significantly higher than those predicted by the GUSAR analysis.

Recently, we reported the synthesis and results of the antimicrobial and antibiofilm assessment of a series of similar *N*-{4-[(4-X-phenyl)sulfonyl]benzoyl}-*L*-valine derivatives (X = H, Cl) [70,71]. The non-substituted analog of **7b**, *N*-[3-methyl-1-oxo-1-(*p*-tolyl)butan-2-yl]-4-(phenylsulfonyl)benzamide presented a better antimicrobial effect compared with **7b** or its chloro-derivative. The increase in the lipophilic character was perhaps detrimental because of the associated lower water solubility. The introduction into the molecule of the bromine atom proved slightly beneficial in the case of the 4*H*-1,3-oxazol-5-one **6**.

Subsequent structural and biological investigations into these kinds of privileged scaffolds can lead to the discovery of new more potent derivatives that can act as optimized candidates for the development of new effective preventive and therapeutic agents. In this respect, we consider three critical positions on the molecular templates that may have an effect on biological action. A first possibility for the future improvement of the antimicrobial property of these analogs is the replacement of the bromine atom in the arylsulfonylphenyl fragment with different substituents, such as fluorine, iodine, trifluoromethyl, or nitro. For this purpose, other benzene analogs are used as starting molecules in the Friedel–Crafts sulfonylation reaction. As a second optimization choice, in the *N*-acylation reaction instead of *L*-valine, we consider the use of other natural or unnatural α-amino acids (such as histidine and tryptophan) or the incorporation of several α-amino acid residues in the molecules as it is well-known that some natural polypeptides bearing the 1,3-oxazole ring (e.g., microcin B17) are inhibitors of DNA-gyrase [3]. The use of other aromatic compounds with different substituents (e.g., I, NO_2, CF_3, OCH_3) in the reaction with **6** is the third alternative route of synthesis to enhance the biological activity of these molecular scaffolds. The iodine atom is more active than other halogens, CF_3-functionalized compounds showed higher antibacterial activity than those with a CH_3 group, hydrophobic substituents (e.g., benzyloxy, *tert*-butyl) [72], or electron-withdrawing groups (such as nitro) on aromatic cores increased the antibacterial effect [73], small substituents (e.g., hydroxy) at 4-position of the

phenyl nucleus improved the antibacterial potency [62]. In addition, it was noticed that the electron-donating substituents (such as OCH_3) on the aromatic moiety enhanced the antioxidant activity compared with the electron-withdrawing groups and that, in general, this pharmacological action increases with the increasing electron-donating effect of the substituent [74–77].

4. Materials and Methods

4.1. Prediction of the Molecular Mechanism of Action and Toxicity

4.1.1. Structure-Based Similarity Analysis

Each target structure was inputted into the search engine of the ChEMBL database [78] and a similarity search was performed using a 50% threshold. The output structures were extracted together with any associated data of biological activity on bacteria. The DataWarrior v5.2.1 software (Actelion Pharmaceuticals Ltd., Allschwil, Switzerland, https://openmolecules.org/) [79] was used to filter the duplicate structures and to calculate the clogP values.

4.1.2. PASS Prediction

The web-based Prediction of Activity Spectra for Substances (PASS) application was used to evaluate the antimicrobial potential of the newly designed bromo derivatives based on their chemical structures. The array of results was analyzed for any effect with a predicted Pa value higher than the Pi value.

4.2. General Information

Melting points (mp) (in °C), were determined on a Boëtius hot plate microscope (VEB Wägetechnik Rapido, PHMK 81/3026, Radebeul, Germany) and are reported uncorrected. UV/VIS spectra were recorded for solutions of the new compounds in methanol at concentration of ≈0.025 mM and in acetonitrile at ≈0.015 mM on an Analytik Jena Specord 40 ultraviolet/visible spectrophotometer (Analytik Jena AG, Jena, Germany) using a quartz cuvette with a path length of 1.00 cm. Values of the wavelength (corresponding to the maximum absorbance), λ_{max} (in nm), and of the logarithm to the base 10 of the molar absorption coefficient, ε_{max} ($M^{-1} \cdot cm^{-1}$) are provided. FTIR spectra were collected with a Bruker Optics Vertex 70 Fourier-transform infrared spectrophotometer (Bruker Optics GmbH, Ettlingen, Germany) using the conventional KBr pellet technique. The position of the selected absorption bands in the FTIR spectra is reported using the wavenumber at the absorption maximum, $\widetilde{\nu}_{max}$ (in cm^{-1}). The intensity of the FTIR peaks is provided as very strong (vs); strong (s); medium (m); and weak (w). Nuclear magnetic resonance spectra were registered on a Varian Gemini 300 BB NMR spectrometer (Varian, Inc., Palo Alto, CA, USA) operating at 300 MHz for ^{1}H NMR and 75 MHz for ^{13}C NMR, in deuterated solvents, i.e., dimethyl sulfoxide-d_6 (DMSO-d_6) or deuterochloroform ($CDCl_3$). Additional evidence was provided by the 2D HETCOR and COSY experiments. Chemical shifts, δ, were measured in ppm with respect to the ^{1}H or ^{13}C resonance of $(CH_3)_4Si$ (tetramethylsilane, TMS), and the coupling constants, J, are expressed in Hz. The multiplicity of ^{1}H NMR signals is provided as per the following convention: singlet (s); doublet (d); doublet of doublets (dd); triplet (t); triplet of triplets (tt); septet (sept); septet of doublets (septd); octet (oct); multiplet (m); and broad (br). Proton NMR spectroscopic data are quoted in the following order: ^{1}H chemical shift, multiplicity, proton number, signal/hydrogen atom assignment, coupling constants, and ^{13}C NMR spectroscopic data are reported as follows: δ_C-value, signal/carbon atom attribution. GC/EI–MS data were acquired on a Fisons Instruments GC 8000 series gas chromatograph coupled to an MD 800 mass spectrometer detector equipped with an electron ionization source and with a quadrupole mass analyzer (Fisons Instruments SpA, Rodano, Milano, Italy), using an SLB-5ms capillary column (d_f 0.25 µm; L × I.D. 30 m × 0.32 mm), CH_2Cl_2 as solvent, and a flow rate of helium carrier gas of 2 mL/min. Reversed-phase high-performance liquid chromatography (HPLC) was performed on a Beckman Coulter System Gold 126 liquid chromatograph, equipped with a

System Gold 166 UV/VIS spectrophotometer detector (Beckman Coulter, Inc., Fullerton, CA, USA), a Rheodyne injection system, and a LiChrosorb RP-18 column (d_p 5 μm; L × I.D. 25 cm × 4.6 mm). The flow rate of eluent, a mixture of CH_3OH–H_2O in different volume ratios, was 1 mL/min. The compounds' purities (%) and retention times, t_R (in min), were reported. Elemental analysis was carried out on a Costech ECS 4010 instrument (Costech Analytical Technologies Inc., Valencia, CA, USA).

4.3. Chemistry

The chemicals and reagents were obtained from commercial sources of analytical grade and were used as received, except for CH_2Cl_2 which was dried over anhydrous $CaCl_2$.

4.3.1. Preparation and Characterization of 2-{4-[(4-Bromophenyl)sulfonyl]benzamido}-3-methylbutanoic Acid **5**

The solution of 2.34 g (20 mmol) of *L*-valine in 20 mL (0.80 g, 20 mmol) of 1 N NaOH solution was cooled at 0–5 °C in an ice bath and then two other solutions were added simultaneously in droplets under magnetic stirring during half an hour, namely a solution of 7.19 g (20 mmol) of crude 4-[(4-bromophenyl)sulfonyl]benzoyl chloride **4** in 45 mL of anhydrous dichloromethane, and a 2 N NaOH solution (10 mL, 0.80 g, 20 mmol). The reaction mixture was stirred for another 1 h at room temperature and then the separated aqueous phase was acidified with 2 N HCl when a white precipitate appeared. The solid was filtered off at low-pressure, washed thoroughly with distilled water on the filter to remove traces of hydrochloric acid, air-dried, and recrystallized from water when white acicular crystals resulted.

Yield 94% (8.28 g, 18.80 mmol). mp 194–196 °C.

UV/VIS (CH_3OH) λ_{max} nm ($\log_{10} \varepsilon_{max}$): 202.6 (4.48); 252.0 (4.20); (CH_3CN) λ_{max} nm ($\log_{10} \varepsilon_{max}$): 196.2 (4.83); 228.2 (4.36); 252.2 (4.57).

FTIR (KBr disc) $\widetilde{\nu}_{max}$ cm^{-1}: 3347 s (νN–H); 3300–2500 vs (νO–H); 3092 s; 3069 s (νC–H, aromatic); 2966 vs ($\nu_{asym}CH_3$); 2933 s (νC–H, aliphatic); 2876 s ($\nu_{sym}CH_3$); 2676 m; 2599 m (combination bands); 1746 vs (νO=C–O); 1635 vs (νO=C–N, amide I); 1599 s; 1573 vs; 1487 s; 1467 s (νC=C, aromatic); 1536 vs (δN–H, amide II); 1324 vs; 1296 vs; 1281 vs ($\nu_{asym}SO_2$); 1161 vs ($\nu_{sym}SO_2$); 852 s (γC–H, aromatic); 613 vs; and 575 vs (νC–Br).

^{1}H NMR (300 MHz, DMSO-d_6) δ ppm: 8.73 (d, 1H, H-3, J = 8.0 Hz); 8.08 (d, 2H, H-7, H-11, J = 8.8 Hz); 8.04 (d, 2H, H-8, H-10, J = 8.8 Hz); 7.92 (d, 2H, H-13, H-17, J = 8.8 Hz); 7.85 (d, 2H, H-14, H-16, J = 8.8 Hz); 4.29 (dd, 1H, H-4, J = 8.1, 6.9 Hz); 2.17 (oct, 1H, H-18, J = 6.9 Hz); 0.95 (d, 3H, H-19, J = 6.9 Hz); and 0.94 (d, 3H, H-20, J = 6.9 Hz).

^{13}C NMR (75 MHz, DMSO-d_6) δ ppm: 172.79 (C-5); 165.78 (C-2); 142.66 (C-9); 139.92 (C-12); 139.03 (C-6); 132.96 (C-14, C-16); 129.48 (C-7, C-11); 129.08 (C-8, C-10); 128.22 (C-15); 127.49 (C-13, C-17); 58.43 (C-4); 29.48 (C-18); 19.25 (C-19); and 18.61 (C-20).

Reversed-phase HPLC (CH_3OH–H_2O 30:70, V/V; flow rate 1 mL/min; λ 250 nm): purity 99.99%; t_R 4.47 min.

Elem. anal. (%) found: C, 49.06; H, 4.11; N, 3.19; and S, 7.28; calcd. for $C_{18}H_{18}BrNO_5S$ (M_r 440.31): C, 49.10; H, 4.12; N, 3.18; and S, 7.28.

4.3.2. Preparation and Characterization of 2-{4-[(4-Bromophenyl)sulfonyl]phenyl}-4-isopropyl-4*H*-1,3-oxazol-5-one **6**

An amount of 4.62 g (10.5 mmol) of **5** was suspended under magnetic stirring at room temperature in 50 mL of dry CH_2Cl_2 and then an equimolar quantity (1.15 mL, 1.06 g, 10.5 mmol) of 4-methylmorpholine was added. A volume of 1 mL (1.14 g, 10.5 mmol) of ethyl chloroformate was added dropwise with continuous stirring to the solution obtained above. The reaction mixture was stirred for an additional 30 min and further poured into 100 mL of ice water. The separated organic phase was washed with 5% $NaHCO_3$ solution, then with distilled water and dried ($MgSO_4$). After concentration under low-pressure, solid product **6** was recrystallized from cyclohexane when white crystals were obtained.

Yield 90% (3.99 g, 9.45 mmol). mp 144–145 °C.

UV/VIS (CH_3OH) λ_{max} nm ($\log_{10} \varepsilon_{max}$): 202.6 (4.49); 227.3 (4.14); 252.0 (4.35); (CH_3CN) λ_{max} nm ($\log_{10} \varepsilon_{max}$): 197.1 (4.93); 229.1 (4.48); 252.2 (4.64).

FTIR (KBr disc) $\widetilde{\nu}_{max}$ cm^{-1}: 3092 m; 3067 w (νC–H, aromatic); 2963 m ($\nu_{asym}CH_3$); 2930 m (νC–H, aliphatic); 2875 m ($\nu_{sym}CH_3$); 1825 vs (νC=O); 1650 vs (νC=N); 1599 w; 1573 s; 1469 m (νC=C, aromatic); 1329 vs; 1293 s ($\nu_{asym}SO_2$); 1243 m (ν_{asym}C–O–C); 1160 vs ($\nu_{sym}SO_2$); 1040 vs (ν_{sym}C–O–C); 845 m (γC–H, aromatic); 614 vs; and 574 s (νC–Br).

^{1}H NMR (300 MHz, $CDCl_3$) δ ppm: 8.16 (d, 2H, H-7, H-11, J = 8.5 Hz); 8.05 (d, 2H, H-8, H-10, J = 8.5 Hz); 7.83 (d, 2H, H-13, H-17, J = 8.5 Hz); 7.68 (d, 2H, H-14, H-16, J = 8.5 Hz); 4.32 (d, 1H, H-4, J = 4.7 Hz); 2.40 (septd, 1H, H-18, J = 6.9, 4.7 Hz); 1.14 (d, 3H, H-19, J = 6.9 Hz); and 0.99 (d, 3H, H-20, J = 6.9 Hz).

^{13}C NMR (75 MHz, $CDCl_3$) δ ppm: 176.98 (C-5); 160.36 (C-2); 144.89 (C-9); 139.92 (C-12); 132.97 (C-14, C-16); 130.58 (C-6); 129.49 (C-13, C-17); 129.23 (C-15); 128.99 (C-7, C-11); 128.19 (C-8, C-10); 71.04 (C-4); 31.42 (C-18); 18.90 (C-19); and 17.65 (C-20).

GC/EI–MS (70 eV) m/z (rel. abund. %): 379 (^{79}Br)/381 (^{81}Br) (71.61/100, BP) [M-C_3H_6]$^+$; 323/325 (41.31/38.56) [$^{79}BrC_6H_4SO_2C_6H_4CHNH]^+$/[$^{81}BrC_6H_4SO_2C_6H_4CHNH]^+$ or [$^{79}BrC_6H_4SO_2C_6H_4CO]^+$/[$^{81}BrC_6H_4SO_2C_6H_4CO]^+$; 207 (29.87); 203 (40.89) [$^{79}BrC_6H_4SO]^+$; 76 (24.15) [$C_6H_4]^+$; 43 (37.71) [$C_3H_7]^+$; and t_R 36.53 min.

Reversed-phase HPLC (CH_3OH–H_2O 60:40, V/V; flow rate 1 mL/min; λ 250 nm): purity 94.16%; t_R 4.05 min.

Elem. anal. (%) found: C, 51.24; H, 3.81; N, 3.33; and S, 7.57; calcd. for $C_{18}H_{16}BrNO_4S$ (M_r 422.29): C, 51.19; H, 3.82; N, 3.32; and S, 7.59.

4.3.3. General Procedure for the Preparation of 2-Acylamino Ketones **7a**,**b** and Their Characterization

To a solution of raw 2-{4-[(4-bromophenyl)sulfonyl]phenyl}-4-isopropyl-4*H*-1,3-oxazol-5-one **6** (2.11 g, 5 mmol) in 25 mL of anhydrous arene (i.e., benzene and toluene, respectively), 2.00 g (15 mmol) of anhydrous aluminum trichloride were added portion-wise with magnetic stirring at room temperature. The reaction mixture was stirred for a further 20 h until hydrogen chloride emission ceased and then poured into 100 mL of ice water acidified with 5 mL of 37% HCl. A precipitate was obtained, which was isolated by filtration, washed on the filter with cold distilled water, and further with a cold ethanol/distilled water (1:1, V/V) mixture. The aqueous filtrate was extracted with CH_2Cl_2 (2 × 15 mL), then the organic phase was washed with distilled water, dried (Na_2SO_4), and concentrated to dryness by vacuum distillation, when the second fraction of **7** was isolated. Purification of the crude product by recrystallization from ethanol afforded colorless crystals.

4-[(4-Bromophenyl)sulfonyl]-*N*-(3-methyl-1-oxo-1-phenylbutan-2-yl)benzamide **7a**

Compound **7a** was synthesized by the reaction of **6** with benzene (25 mL, 21.85 g, 279.7 mmol).

Yield 80% (2.00 g, 4.00 mmol). mp 164–166 °C.

UV/VIS (CH_3OH) λ_{max} nm ($\log_{10} \varepsilon_{max}$): 202.6 (4.49); 252.0 (4.19); (CH_3CN) λ_{max} nm ($\log_{10} \varepsilon_{max}$): 198.0 (5.03); 250.2 (4.77).

FTIR (KBr disc) $\widetilde{\nu}_{max}$ cm^{-1}: 3301 s (νN–H); 3089 m; 3061 m; 3040 m (νC–H, aromatic); 2962 m ($\nu_{asym}CH_3$); 2931 m (νC–H, aliphatic); 2872 m ($\nu_{sym}CH_3$); 1655 vs (ν<u>O=C</u>–O and ν<u>O=C</u>–N, amide I; overlapped); 1597 m; 1574 s; 1483 m; 1469 m; 1448 m (νC=C, aromatic); 1528 s (δN–H, amide II); 1323 vs; 1289 s ($\nu_{asym}SO_2$); 1161 vs ($\nu_{sym}SO_2$); 854 m (γC–H, aromatic); 615 vs; and 580 s (νC–Br).

^{1}H NMR (300 MHz, DMSO-d_6) δ ppm: 8.99 (d, 1H, H-3, J = 8.0 Hz); 8.05 (m, 6H, H-7, H-8, H-10, H-11, H-22, H-26); 7.91 (d, 2H, H-13, H-17, J = 8.5 Hz); 7.84 (d, 2H, H-14, H-16, J = 8.5 Hz); 7.64 (br t, 1H, H-24, J = 7.6 Hz); 7.53 (br t, 2H, H-23, H-25, J = 7.6 Hz); 5.38 (t, 1H, H-4, J = 7.7 Hz); 2.28 (m, 1H, H-18); 0.92 (d, 3H, H-19, J = 7.1 Hz); and 0.90 (d, 3H, H-20, J = 7.1 Hz).

^{13}C NMR (75 MHz, DMSO-d_6) δ ppm: 199.19 (C-5); 165.57 (C-2); 142.76 (C-9); 139.88 (C-12); 138.78 (C-6); 136.17 (C-21); 133.44 (C-24); 132.94 (C-14, C-16); 129.48 (C-13, C-17);

129.04 (C-7, C-11); 128.82 (C-23, C-25); 128.24 (C-22, C-26); 128.22 (C-15); 127.53 (C-8, C-10); 59.23 (C-4); 29.50 (C-18); 19.72 (C-19); and 18.36 (C-20).

Reversed-phase HPLC (CH_3OH–H_2O 60:40, V/V; flow rate 1 mL/min; λ 250 nm): purity 92.02%; t_R 4.35 min.

Elem. anal. (%) found: C, 57.63; H, 4.41; N, 2.81; and S, 6.40; calcd. for $C_{24}H_{22}BrNO_4S$ (M_r 500.40): C, 57.60; H, 4.43; N, 2.80; and S, 6.41.

4-[(4-Bromophenyl)sulfonyl]-*N*-[3-methyl-1-oxo-1-(*p*-tolyl)butan-2-yl]benzamide **7b**

Compound **7b** was synthesized by the reaction of **6** with toluene (25 mL, 21.63 g, 234.8 mmol).

Yield 86% (2.21 g, 4.30 mmol). mp 154–155 °C.

UV/VIS (CH_3OH) λ_{max} nm ($\log_{10} \varepsilon_{max}$): 202.6 (4.47); 255.5 (4.18); (CH_3CN) λ_{max} nm ($\log_{10} \varepsilon_{max}$): 197.8 (5.01); 254.8 (4.78).

FTIR (KBr disc) $\widetilde{\nu}_{max}$ cm^{-1}: 3281 s (νN–H); 3086 m; 3058 m; 3037 m (νC–H, aromatic); 2962 m ($\nu_{asym}CH_3$); 2929 m (νC–H, aliphatic); 2868 m ($\nu_{sym}CH_3$); 1655 vs (νO=C–O and νO=C–N, amide I; overlapped); 1606 m; 1572 s; 1483 m; 1467 m (νC=C, aromatic); 1530 s (δN–H, amide II); 1325 s; 1305 m; 1287 m ($\nu_{asym}SO_2$); 1161 vs ($\nu_{sym}SO_2$); 858 m (γC–H, aromatic); 617 s; and 576 s (νC–Br).

^{1}H NMR (300 MHz, DMSO-d_6) δ ppm: 8.94 (d, 1H, H-3, J = 8.0 Hz); 8.06 (d, 2H, H-7, H-11, J = 8.8 Hz); 8.03 (d, 2H, H-8, H-10, J = 8.8 Hz); 7.95 (d, 2H, H-22, H-26, J = 8.2 Hz); 7.91 (d, 2H, H-13, H-17, J = 8.8 Hz); 7.84 (d, 2H, H-14, H-16, J = 8.8 Hz); 7.33 (d, 2H, H-23, H-25, J = 8.2 Hz); 5.36 (t, 1H, H-4, J = 7.7 Hz); 2.36 (s, 3H, CH_3); 2.27 (m, 1H, H-18); 0.92 (d, 3H, H-19, J = 7.4 Hz); and 0.89 (d, 3H, H-20, J = 7.4 Hz).

^{13}C NMR (75 MHz, DMSO-d_6) δ ppm: 198.57 (C-5); 165.47 (C-2); 143.89 (C-24); 142.72 (C-9); 139.88 (C-12); 138.81 (C-6); 133.61 (C-21); 132.92 (C-14, C-16); 129.44 (C-13, C-17); 129.34 (C-23, C-25); 129.00 (C-7, C-11); 128.36 (C-22, C-26); 128.18 (C-15); 127.49 (C-8, C-10); 59.05 (C-4); 29.56 (C-18); 21.12 (CH_3); 19.71 (C-19); and 18.33 (C-20).

Reversed-phase HPLC (CH_3OH–H_2O 60:40, V/V; flow rate 1 mL/min; λ 250 nm): purity 99.99%; t_R 4.95 min.

Elem. anal. (%) found: C, 58.34; H, 4.69; N, 2.71; and S, 6.21; calcd. for $C_{25}H_{24}BrNO_4S$ (M_r 514.43): C, 58.37; H, 4.70; N, 2.72; and S, 6.23.

4.3.4. General Procedure for the Preparation of 2,5-Disubstituted 4-Isopropyl-1,3-oxazoles **8a**,**b** and Their Characterization

A mixture of 10 mmol of crude **7** and 20 mL (33.40 g, 217.8 mmol) of phosphoryl trichloride was heated under reflux during 4 h. The excess phosphoryl trichloride was evaporated under reduced pressure. The resulting oily residue was cooled, treated with an ice water mixture, and extracted with 2 × 20 mL CH_2Cl_2. The organic phase was separated and washed with 5% $NaHCO_3$ solution, then with distilled water and dried (Na_2SO_4). The solvent was evaporated off under vacuum. Purification of the resulting solid was performed by recrystallization from ethanol when colorless crystals of **8** were obtained.

2-{4-[(4-Bromophenyl)sulfonyl]phenyl}-4-isopropyl-5-phenyl-1,3-oxazole **8a**

Compound **8a** was synthesized from 5.00 g (10 mmol) of 2-acylamino ketone **7a**.

Yield 94% (4.53 g, 9.39 mmol). mp 165–167 °C.

UV/VIS (CH_3OH) λ_{max} nm ($\log_{10} \varepsilon_{max}$): 202.6 (4.48); 249.3 (4.10); 333.9 (4.13); (CH_3CN) λ_{max} nm ($\log_{10} \varepsilon_{max}$): 196.2 (4.95); 248.6 (4.56); 335.6 (4.64).

FTIR (KBr disc) $\widetilde{\nu}_{max}$ cm^{-1}: 3092 m; 3063 m; 3041 w (νC–H, aromatic); 2963 s ($\nu_{asym}CH_3$); 2930 m (νC–H, aliphatic); 2869 m ($\nu_{sym}CH_3$); 1602 m (νC=N); 1588 m; 1574 s; 1543 w; 1494 m; 1471 m; 1446 m (νC=C, aromatic); 1323 vs; 1293 m ($\nu_{asym}SO_2$); 1280 m (ν_{asym}C–O–C); 1155 vs ($\nu_{sym}SO_2$); 1099 s (ν_{sym}C–O–C); 844 m (γC–H, aromatic); 617 s; and 568 s (νC–Br).

^{1}H NMR (300 MHz, $CDCl_3$) δ ppm: 8.22 (d, 2H, H-7, H-11, J = 8.8 Hz); 8.00 (d, 2H, H-8, H-10, J = 8.8 Hz); 7.82 (d, 2H, H-13, H-17, J = 8.8 Hz); 7.65 (d, 2H, H-14, H-16, J = 8.8 Hz); 7.64

(dd, 2H, H-22, H-26, *J* = 7.4, 1.4 Hz); 7.48 (br t, 2H, H-23, H-25, *J* = 7.4 Hz); 7.37 (tt, 1H, H-24, *J* = 7.4, 1.4 Hz); 3.29 (sept, 1H, H-18, *J* = 6.9 Hz); and 1.36 (d, 6H, H-19, H-20, *J* = 6.9 Hz).

^{13}C NMR (75 MHz, $CDCl_3$) δ ppm: 157.78 (C-2); 145.47 (C-5); 144.19 (C-4); 141.71 (C-12); 140.56 (C-9); 132.80 (C-14, C-16); 132.33 (C-6); 129.29 (C-13, C-17); 129.01 (C-23, C-25); 128.81 (C-21); 128.78 (C-15); 128.39 (C-24); 128.26 (C-7, C-11); 127.09 (C-8, C-10); 126.25 (C-22, C-26); 26.10 (C-18); and 22.07 (C-19, C-20).

Reversed-phase HPLC (CH_3OH–H_2O 70:30, *V*/*V*; flow rate 1 mL/min; λ 335 nm): purity 98.95%; t_R 5.97 min.

Elem. anal. (%) found: C, 59.71; H, 4.18; N, 2.91; and S, 6.67; calcd. For $C_{24}H_{20}BrNO_3S$ (M_r 482.39): C, 59.76; H, 4.18; N, 2.90; and S, 6.65.

2-{4-[(4-Bromophenyl)sulfonyl]phenyl}-4-isopropyl-5-(*p*-tolyl)-1,3-oxazole **8b**

Compound **8b** was synthesized from 5.14 g (10 mmol) of 2-acylamino ketone **7b**.

Yield 91% (4.52 g, 9.10 mmol). mp 215–217 °C.

UV/VIS (CH_3OH) λ_{max} nm ($\log_{10}\varepsilon_{max}$): 202.6 (4.48); 249.3 (4.11); 337.4 (4.09); (CH_3CN) λ_{max} nm ($\log_{10}\varepsilon_{max}$): 195.3 (4.96); 249.5 (4.59); 340.1 (4.64).

FTIR (KBr disc) $\tilde{\nu}_{max}$ cm^{-1}: 3091 m; 3069 w; 3028 w (νC–H, aromatic); 2963 m ($\nu_{asym}CH_3$); 2925 m (νC–H, aliphatic); 2869 m ($\nu_{sym}CH_3$); 1601 m (νC=N); 1592 m; 1574 m; 1545 w; 1508 m; 1471 m (νC=C, aromatic); 1322 s; 1292 m ($\nu_{asym}SO_2$); 1280 m (ν_{asym}C–O–C); 1156 vs ($\nu_{sym}SO_2$); 1097 s (ν_{sym}C–O–C); 846 m (γC–H, aromatic); 617 s; and 568 s (νC–Br).

^{1}H NMR (300 MHz, $CDCl_3$) δ ppm: 8.21 (d, 2H, H-7, H-11, *J* = 8.5 Hz); 8.00 (d, 2H, H-8, H-10, *J* = 8.5 Hz); 7.82 (d, 2H, H-13, H-17, *J* = 8.5 Hz); 7.65 (d, 2H, H-14, H-16, *J* = 8.5 Hz); 7.53 (d, 2H, H-22, H-26, *J* = 8.2 Hz); 7.28 (d, 2H, H-23, H-25, *J* = 8.2 Hz); 3.26 (sept, 1H, H-18, *J* = 6.9 Hz); 2.41 (s, 3H, CH_3); and 1.35 (d, 6H, H-19, H-20, *J* = 6.9 Hz).

^{13}C NMR (75 MHz, $CDCl_3$) δ ppm: 157.52 (C-2); 145.69 (C-5); 143.63 (C-4); 141.57 (C-12); 140.61 (C-9); 138.48 (C-24); 132.80 (C-14, C-16); 132.43 (C-6); 129.70 (C-23, C-25); 129.29 (C-13, C-17); 128.76 (C-15); 128.25 (C-7, C-11); 127.03 (C-8, C-10); 126.22 (C-22, C-26); 126.01 (C-21); 26.08 (C-18); 22.07 (C-19, C-20); and 21.47 (CH_3).

Reversed-phase HPLC (CH_3OH–H_2O 70:30, *V*/*V*; flow rate 1 mL/min; λ 335 nm): purity 99.99%; t_R 7.32 min.

Elem. anal. (%) found: C, 60.52; H, 4.46; N, 2.81; and S, 6.48; calcd. for $C_{25}H_{22}BrNO_3S$ (M_r 496.42): C, 60.49; H, 4.47; N, 2.82; and S, 6.46.

4.4. Assessment of Antimicrobial Activity

The evaluation of the influence of the compounds on microbial growth and biofilm formation was performed using an adapted disk diffusion assay, the standard broth microdilution method, and the microtiter plate test [80].

4.4.1. Pathogenic Microbial Strains

The pathogenic microorganisms tested included three Gram-positive bacteria, i.e., *B. subtilis* 6683, *E. faecium* E5, *S. aureus* ATCC 6538, and two Gram-negative bacteria, namely *E. coli* ATCC 8739, *P. aeruginosa* ATCC 27853, as well as a fungal *C. albicans* 393 strain.

4.4.2. Agar Diffusion Assay

The antimicrobial activity was screened using an adapted agar diffusion method [81]. Briefly, the bacterial and fungal suspensions were prepared in phosphate-buffered saline from fresh microbial cultures and their density was adjusted to 0.5 McFarland. The compounds were dissolved in DMSO at a concentration of 5 mg/mL and then a volume of 5 µL was spotted on the inoculated plates. The diameters of the growth inhibition zones were measured after incubation for 24 h at 37 °C. Standardized discs of ciprofloxacin, 5 µg (Oxoid), and fluconazole, 25 µg (Oxoid) were used as positive controls.

4.4.3. Evaluation of the Effects of the Tested Compounds on the Antibiotic Susceptibility Profile

Standardized microbial suspensions of *E. faecium* E5 and *S. aureus* ATCC 6538 were put in contact with subinhibitory concentrations (0.25 mg/mL) of tested compounds **5** and **6** prepared in broth. After incubation at 37 °C for 24 h, the bacterial cultures were used to evaluate their antibiotic susceptibility profile. The disk diffusion method was performed to assess the susceptibility to the following antibiotics: ampicillin, linezolid, penicillin, vancomycin for Gram-positive *E. faecium* E5 strain and azithromycin, cefoxitin, clindamycin, linezolid, penicillin, rifampicin, trimethoprim-sulfamethoxazole, and vancomycin (bioMérieux, Paris, France) for Gram-positive *S. aureus* ATCC 6538 strain. The reading of the results was performed following the Clinical and Laboratory Standards Institute (CLSI, Berwyn, PA, USA) guidelines.

4.4.4. Broth Microdilution Assay

The standard broth microdilution test was performed on 96-well microtiter plates. The compounds were solubilized in DMSO at a concentration of 10 mg/mL. Serial dilutions of the tested compounds were prepared in sterile broth and the obtained solutions of different concentrations were inoculated with each standardized microbial suspension. Ciprofloxacin and fluconazole (Oxoid) served as positive controls. After incubation for 24 h at 37 °C, the MIC values were determined as the lowest concentration of compound required to inhibit the microbial growth, as detected spectrophotometrically (Apollo LB 911 ELISA Reader, Berthold Technologies GmbH & Co. KG, Waltham, MA, USA) [82]. The assays were performed in triplicate.

4.4.5. Microplate Microtiter Assay

The influence of the compounds on the biofilm formation was determined using the microtiter plate assay. Briefly, after the determination of the MIC values, the microplates were emptied and washed three times with sterile distilled water for the removal of planktonic microbial cells. The biofilms adherent on the plastic wells were fixed with methanol for 5 min and stained with 1% crystal violet solution for a quarter of an hour. The excess dye was removed and thereafter the fixed dye was resuspended in 33% acetic acid. Ciprofloxacin (Oxoid) was used as a positive control for antibacterial tests and fluconazole (Oxoid) for antifungal testing. The absorbance of the colored solutions was recorded with an ELISA Reader (Apollo LB 911). The minimal biofilm inhibitory concentration (MBIC), defined as the lowest compound concentration required to inhibit biofilm formation, was determined. The results from three separate biological replicates were mediated [83].

4.5. Evaluation of Antioxidant Activity

The antioxidant activity of newly obtained derivatives **5**–**8** was studied spectrophotometrically by means of the DPPH, ABTS, and ferric reducing power methods [84–86].

4.5.1. Antioxidant Activity Assay by DPPH Method

The antioxidant effect of new compounds was determined according to the well-known DPPH assay based on the fact that the antioxidant samples react with stable 2,2-diphenyl-1-(2,4,6-trinitrophenyl)hydrazin-1-yl (2,2-diphenyl-1-picrylhydrazyl, DPPH), an effective free radical trap with an absorption band at 517 nm, which converts to its reduced form, i.e., 1,1-diphenyl-2-(2,4,6-trinitrophenyl)hydrazine (2,2-diphenyl-1-picryl hydrazine), with a color change from purple to yellow accompanied by a decrease in absorption at 517 nm [84].

The antioxidant potential of the tested compounds was investigated according to the method previously described by Blois [87–89], with some modifications, and compared with the free radical scavenging activity of AA, BHA, and BHT standards.

Briefly, 2 mL of a solution of DPPH in ethanol at a concentration of 400 μM was added to 2 mL of each solution of the tested compound in DMSO at a concentration of 500 μM. After maintaining the samples in the dark at room temperature for 30 min, the absorbance of each sample at the wavelength of 517 nm was measured on a Specord 40 UV/VIS

spectrophotometer (Analytik Jena AG, Jena, Germany). Then, the radical scavenging activity (*RSA*) in percent (%) was calculated using the following formula:

$$RSA\ (\%) = (1 - \frac{A_{\text{sample}} - A_{\text{blank sample}}}{A_{\text{DPPH control}}}) \times 100$$

where A_{sample} is the absorbance of the tested compound solution with the DPPH solution, $A_{\text{blank sample}}$ is the absorbance of the tested compound solution (without the DPPH solution), and $A_{\text{DPPH control}}$ is the absorbance of the DPPH solution (without the tested compound solution) [90]. Each analysis was performed on three replicates and the results were averaged.

4.5.2. Antioxidant Activity Assay by ABTS Method

The ABTS discoloration test is based on the ability of the antioxidant agents to scavenge the long-life ABTS radical-cation, $ABTS^{\bullet+}$ [91]. The stable green-blue radical-cationic chromophore, $ABTS^{\bullet+}$, which has an absorption maximum at the wavelength of 734 nm, by reaction with most antioxidants turns into its colorless neutral form, i.e., 2,2′-azino-bis(3-ethylbenzothiazoline-6-sulfonic acid) (ABTS) [85].

The antioxidant capacity of the tested compounds was assessed as described earlier by Re et al. [91], with some modifications. The $ABTS^{\bullet+}$ is prepared by oxidation of ABTS with radical-initiator potassium persulfate. Initially, the stock solution of ABTS was obtained by dissolving it in water at a concentration of 7 μM. The ABTS radical cation ($ABTS^{\bullet+}$) was then generated by reacting the 7 μM ABTS stock solution with a 2.45 μM $K_2S_2O_8$ solution (1:1, V/V) and kept in the dark at room temperature for 12–16 h. Before analysis, this solution was diluted with ethanol and equilibrated at 30 °C to have absorbance at 734 nm, A_{734} of 0.7000 ± 0.02. Subsequently, 2 mL of $ABTS^{\bullet+}$ solution was added to 2 mL of 500 μM tested compound solution in DMSO. After 6 min, the absorbance of each sample was read at 734 nm with a UV/VIS spectrophotometer (Specord 40, Analytik Jena AG, Jena, Germany) and converted into the percentage radical scavenging activity, %*RSA*, using the formula:

$$RSA\ (\%) = (1 - \frac{A_{\text{sample}} - A_{\text{blank sample}}}{A_{\text{ABTS}^{\bullet+}\text{ control}}}) \times 100$$

where A_{sample} is the absorbance of the tested compound solution with the $ABTS^{\bullet+}$ solution, $A_{\text{blank sample}}$ is the absorbance of the tested compound solution (without the $ABTS^{\bullet+}$ solution), and $A_{\text{ABTS}^{\bullet+}\text{ control}}$ is the absorbance of the $ABTS^{\bullet+}$ solution (without the tested compound solution) [89,90]. All determinations were undertaken in triplicate and the results were averaged. The same antioxidant agents (AA, BHA, and BHT) were used as positive controls.

4.5.3. Ferric Reducing Power Assay

In the ferric reducing power test, is measured the reduction in the bright red color potassium ferricyanide to the intense blue color ferric ferrocyanide (Prussian blue), which occurs by means of antioxidants in acidic environments, with an increase in absorbance at 700 nm [84].

The ability of all the newly synthesized compounds to reduce iron(III) to iron(II) was determined by the modified Oyaizu method [92–94]. The sample solutions were prepared in DMSO at a concentration of 500 μM. Two milliliters of each tested compound solution were mixed with 2 mL of 0.2 M phosphate buffer (pH 6.6) and 2 mL of 1% $K_3[Fe(CN)_6]$ solution. After 20 min incubation at 50 °C, 2 mL of 10% trichloroacetic acid solution was added, and the mixture was centrifuged for 15 min at 4500 rpm. Finally, 2 mL of the upper layer was mixed with 2 mL of deionized water and 0.4 mL of 0.1% $FeCl_3$ solution, and after 5 min the absorbance was recorded at 700 nm with an Analytik Jena Specord 40 UV/VIS spectrophotometer. All analyses were performed on three replicates, and the results were averaged and compared with those of antioxidant standards used, i.e., AA, BHA, and BHT.

4.6. Daphnia magna Toxicity Bioassay

In ecotoxicology, the planktonic crustacean *Daphnia magna* Staus is specified for use in the "OECD Guidelines for the Testing of Chemicals". Test No. 202: "*Daphnia* sp., Acute Immobilization Test" is an acute toxicity study, in which young daphnids, aged less than 24 h at the beginning of the test, are exposed to different concentrations of the chemical under test for 48 h and the half-maximal effective concentration (EC_{50}) determined [95].

In this study, the young *D. magna* Straus organisms were selected according to their size from a parthenogenetic culture. All compounds were tested at six concentrations ranging from 2 to 50 µg/mL, in duplicate, with each replicate having 10 individuals. The concentration range was selected based on the compounds' solubilities and a pre-screening bioassay. *L*-Valine, compound **3**, and a 1% DMSO solution were used as controls. All determinations were carried out using the same conditions (25 °C, a long day photoperiod of 16 h light/8 h dark cycle) in a Sanyo MLR-351H climate test chamber (Sanyo, San Diego, CA, USA) [48,96,97]. After 24 and 48 h of exposure, the lethality was evaluated. LC_{50} was calculated for each compound based on interpolating on lethality curves which were obtained using the least square fit method. The 95% confidence intervals (95% CI) were calculated and the goodness of fit was also evaluated. The calculations were performed using GraphPad Prism v5.1 software (GraphPad Software, Inc., La Jolla, CA, USA). The prediction of LC_{50} at 48 h was made using GUSAR online application (Institute of Biomedical Chemistry, Moscow, Russia, http://www.way2drug.com/gusar/) [98].

5. Conclusions

In order to identify new bioactive compounds, we designed and synthesized novel derivatives that incorporate in the same molecule the *N*-acyl-α-amino acid, 4*H*-1,3-oxazol-5-one, 2-acylamino ketone, or 1,3-oxazole template and, a biologically active fragment derived from diphenyl sulfone. The obtained compounds' structures were confirmed on the basis of spectral studies and elemental analysis data. Taken together, the results of the qualitative and quantitative antimicrobial activity evaluation, antioxidant effect assessment, toxicity bioassay, as well as of in silico analysis revealed a promising potential of *N*-acyl-*L*-valine **5** and 2-substituted 4-isopropyl-4*H*-1,3-oxazol-5-one **6** for the development of novel antimicrobial agents to combat infections produced by Gram-positive bacterial strains, and in particular of *E. faecium* biofilm-associated infections.

6. Patents

Patent application no. a 2019 00668: Theodora-Venera Apostol, Ștefania-Felicia Bărbuceanu, Laura Ileana Socea, Ioana Șaramet, Constantin Drăghici, Valeria Rădulescu, Mariana-Carmen Chifiriuc, Luminița Gabriela Măruțescu, Octavian Tudorel Olaru, and George Mihai Nițulescu, 4-Isopropyl-1,3-oxazol-5(4*H*)-one Derivatives Containing a Diaryl sulfonyl Substituent in Position 2 with Antimicrobial Action, published in RO-BOPI No. 9/2021, from 30 september 2021.

Supplementary Materials: The following supporting information can be downloaded at: https://www.mdpi.com/article/10.3390/pr10091800/s1, Figure S1: The ^{1}H NMR spectrum of 2-{4-[(4-bromophenyl)sulfonyl]benzamido}-3-methylbutanoic acid **5**; Figure S2: The ^{13}C NMR spectrum of 2-{4-[(4-bromophenyl)sulfonyl]benzamido}-3-methylbutanoic acid **5**; Figure S3: The 2D HETCOR spectrum of 2-{4-[(4-bromophenyl)sulfonyl]benzamido}-3-methylbutanoic acid **5**; Figure S4: The ^{1}H NMR spectrum of 2-{4-[(4-bromophenyl)sulfonyl]phenyl}-4-isopropyl-4*H*-1,3-oxazol-5-one **6**; Figure S5: The ^{13}C NMR spectrum of 2-{4-[(4-bromophenyl)sulfonyl]phenyl}-4-isopropyl-4*H*-1,3-oxazol-5-one **6**; Figure S6: The 2D HETCOR spectrum of 2-{4-[(4-bromophenyl)sulfonyl]phenyl}-4-isopropyl-4*H*-1,3-oxazol-5-one **6**; Figure S7: The ^{1}H NMR spectrum of 4-[(4-bromophenyl)sulfonyl]-*N*-(3-methyl-1-oxo-1-phenylbutan-2-yl)benzamide **7a**; Figure S8: The ^{13}C NMR spectrum of 4-[(4-bromophenyl)sulfonyl]-*N*-(3-methyl-1-oxo-1-phenylbutan-2-yl)benzamide **7a**; Figure S9: The ^{13}C NMR spectrum of 4-[(4-bromophenyl)sulfonyl]-*N*-(3-methyl-1-oxo-1-phenylbutan-2-yl)benzamide **7a**; Figure S10: The ^{1}H NMR spectrum of 4-[(4-bromophenyl)sulfonyl]-*N*-[3-methyl-1-oxo-1-(*p*-tolyl)butan-2-yl]benzamide **7b**; Figure S11: The ^{13}C NMR spectrum of 4-[(4-bromophenyl)sulfonyl]-*N*-[3-methyl-1-oxo-1-(*p*-

tolyl)butan-2-yl]benzamide **7b**; Figure S12: The 2D COSY spectrum of 4-[(4-bromophenyl)sulfonyl]-*N*-[3-methyl-1-oxo-1-(*p*-tolyl)butan-2-yl]benzamide **7b**; Figure S13: The 2D HETCOR spectrum of 4-[(4-bromophenyl)sulfonyl]-*N*-[3-methyl-1-oxo-1-(*p*-tolyl)butan-2-yl]benzamide **7b**; Figure S14: The ^{1}H NMR spectrum of 2-{4-[(4-bromophenyl)sulfonyl]phenyl}-4-isopropyl-5-phenyl-1,3-oxazole **8a**; Figure S15: The ^{13}C NMR spectrum of 2-{4-[(4-bromophenyl)sulfonyl]phenyl}-4-isopropyl-5-phenyl-1,3-oxazole **8a**; Figure S16: The 2D HETCOR spectrum of 2-{4-[(4-bromophenyl)sulfonyl]phenyl}-4-isopropyl-5-phenyl-1,3-oxazole **8a**; Figure S17: The ^{1}H NMR spectrum of 2-{4-[(4-bromophenyl) sulfonyl]phenyl}-4-isopropyl-5-(*p*-tolyl)-1,3-oxazole **8b**; Figure S18: The ^{13}C NMR spectrum of 2-{4-[(4-bromophenyl)sulfonyl]phenyl}-4-isopropyl-5-(*p*-tolyl)-1,3-oxazole **8b**; Figure S19: The 2D HETCOR spectrum of 2-{4-[(4-bromophenyl)sulfonyl]phenyl}-4-isopropyl-5-(*p*-tolyl)-1,3-oxazole **8b**; Figure S20: The FTIR spectrum of 2-{4-[(4-bromophenyl)sulfonyl]benzamido}-3-methylbutanoic acid **5**; Figure S21: The FTIR spectrum of 2-{4-[(4-bromophenyl)sulfonyl]phenyl}-4-isopropyl-4*H*-1,3-oxazol-5-one **6**; Figure S22: The FTIR spectrum of 4-[(4-bromophenyl)sulfonyl]-*N*-(3-methyl-1-oxo-1-phenylbutan-2-yl)benzamide **7a**; Figure S23: The FTIR spectrum of 4-[(4-bromophenyl)sulfonyl]-*N*-[3-methyl-1-oxo-1-(*p*-tolyl)butan-2-yl]benzamide **7b**; Figure S24: The FTIR spectrum of 2-{4-[(4-bromophenyl)sulfonyl]phenyl}-4-isopropyl-5-phenyl-1,3-oxazole **8a**; Figure S25: The FTIR spectrum of 2-{4-[(4-bromophenyl)sulfonyl]phenyl}-4-isopropyl-5-(*p*-tolyl)-1,3-oxazole **8b**; Figure S26: The UV/VIS spectrum of 2-{4-[(4-bromophenyl)sulfonyl]benzamido}-3-methylbutanoic acid **5** dissolved in methanol at ≈0.025 mM; Figure S27: The UV/VIS spectrum of 2-{4-[(4-bromophenyl)sulfonyl]phenyl}-4-isopropyl-4*H*-1,3-oxazol-5-one **6** dissolved in methanol at ≈0.025 mM; Figure S28: The UV/VIS spectrum of 4-[(4-bromophenyl)sulfonyl]-*N*-(3-methyl-1-oxo-1-phenylbutan-2-yl)benzamide **7a** dissolved in methanol at ≈0.025 mM; Figure S29: The UV/VIS spectrum of 4-[(4-bromophenyl)sulfonyl]-*N*-[3-methyl-1-oxo-1-(*p*-tolyl)butan-2-yl]benzamide **7b** dissolved in methanol at ≈0.025 mM; Figure S30: The UV/VIS spectrum of 2-{4-[(4-bromophenyl)sulfonyl]phenyl}-4-isopropyl-5-phenyl-1,3-oxazole **8a** dissolved in methanol at ≈0.025 mM; Figure S31: The UV/VIS spectrum of 2-{4-[(4-bromophenyl) sulfonyl]phenyl}-4-isopropyl-5-(*p*-tolyl)-1,3-oxazole **8b** dissolved in methanol at ≈ 0.025 mM; Figure S32: The UV/VIS spectrum of 2-{4-[(4-bromophenyl)sulfonyl]benzamido}-3-methylbutanoic acid **5** dissolved in acetonitrile at ≈ 0.015 mM; Figure S33: The UV/VIS spectrum of 2-{4-[(4-bromophenyl) sulfonyl]phenyl}-4-isopropyl-4*H*-1,3-oxazol-5-one **6** dissolved in acetonitrile at ≈0.015 mM; Figure S34: The UV/VIS spectrum of 4-[(4-bromophenyl)sulfonyl]-*N*-(3-methyl-1-oxo-1-phenylbutan-2-yl)benzamide **7a** dissolved in acetonitrile at ≈0.015 mM; m: The UV/VIS spectrum of 4-[(4-bromophenyl)sulfonyl]-*N*-[3-methyl-1-oxo-1-(*p*-tolyl)butan-2-yl]benzamide **7b** dissolved in acetonitrile at ≈0.015 mM; Figure S36: The UV/VIS spectrum of 2-{4-[(4-bromophenyl)sulfonyl]phenyl}-4-isopropyl-5-phenyl-1,3-oxazole **8a** dissolved in acetonitrile at ≈0.015 mM; Figure S37: The UV/VIS spectrum of 2-{4-[(4-bromophenyl)sulfonyl]phenyl}-4-isopropyl-5-(*p*-tolyl)-1,3-oxazole **8b** dissolved in acetonitrile at ≈0.015 mM; Figure S38: The GC/MS spectrum of 2-{4-[(4-bromophenyl)sulfonyl]phenyl}-4-isopropyl-4*H*-1,3-oxazol-5-one **6**; Figure S39: The RP–HPLC chromatogram of 2-{4-[(4-bromophenyl) sulfonyl]benzamido}-3-methylbutanoic acid **5**; Figure S40: The RP–HPLC chromatogram of 2-{4-[(4-bromophenyl)sulfonyl]phenyl}-4-isopropyl-4*H*-1,3-oxazol-5-one **6**; Figure S41: The RP–HPLC chromatogram of 4-[(4-bromophenyl)sulfonyl]-*N*-(3-methyl-1-oxo-1-phenylbutan-2-yl)benzamide **7a**; Figure S42: The RP–HPLC chromatogram of 4-[(4-bromophenyl)sulfonyl]-*N*-[3-methyl-1-oxo-1-(*p*-tolyl)butan-2-yl]benzamide **7b**; Figure S43: The RP–HPLC chromatogram of 2-{4-[(4-bromophenyl) sulfonyl]phenyl}-4-isopropyl-5-phenyl-1,3-oxazole **8a**; Figure S44: The RP–HPLC chromatogram of 2-{4-[(4-bromophenyl)sulfonyl]phenyl}-4-isopropyl-5-(*p*-tolyl)-1,3-oxazole **8b**.

Author Contributions: Conceptualization, T.-V.A.; methodology, T.-V.A., M.C.C., L.-I.S., C.D., O.T.O., G.M.N., D.-C.V., L.G.M., E.M.P., G.S. and S.-F.B.; investigation, T.-V.A., M.C.C., L.-I.S., C.D., O.T.O., G.M.N., D.-C.V., L.G.M., E.M.P., G.S. and S.-F.B.; writing—original draft preparation, T.-V.A., M.C.C., L.-I.S., C.D., O.T.O., G.M.N., D.-C.V., L.G.M., E.M.P., G.S. and S.-F.B.; writing—review and editing, T.-V.A., M.C.C., C.D., O.T.O., G.M.N. and S.-F.B. All authors have read and agreed to the published version of the manuscript.

Funding: This research was funded by the Publish Not Perish Grants at the "Carol Davila" University of Medicine and Pharmacy, Bucharest, Romania.

Institutional Review Board Statement: Not applicable.

Informed Consent Statement: Not applicable.

Data Availability Statement: The datasets used and/or analyzed during the current study are available from the corresponding author upon reasonable request.

Conflicts of Interest: The authors declare no conflict of interest.

References

1. Christaki, E.; Marcou, M.; Tofarides, A. Antimicrobial Resistance in Bacteria: Mechanisms, Evolution, and Persistence. *J. Mol. Evol.* **2020**, *88*, 26–40. [CrossRef] [PubMed]
2. Chen, J.; Lv, S.; Liu, J.; Yu, Y.; Wang, H.; Zhang, H. An Overview of Bioactive 1,3-Oxazole-Containing Alkaloids from Marine Organisms. *Pharmaceuticals* **2021**, *14*, 1274. [CrossRef]
3. Mhlongo, J.T.; Brasil, E.; de la Torre, B.G.; Albericio, F. Naturally Occurring Oxazole-Containing Peptides. *Mar. Drugs* **2020**, *18*, 203. [CrossRef]
4. Zheng, X.; Liu, W.; Zhang, D. Recent Advances in the Synthesis of Oxazole-Based Molecules via van Leusen Oxazole Synthesis. *Molecules* **2020**, *25*, 1594. [CrossRef] [PubMed]
5. Kakkar, S.; Narasimhan, B. A comprehensive review on biological activities of oxazole derivatives. *BMC Chem.* **2019**, *13*, 16. [CrossRef] [PubMed]
6. Li, Q.; Seiple, I.B. Modular Synthesis of Streptogramin Antibiotics. *Synlett* **2021**, *32*, 647–654. [CrossRef] [PubMed]
7. Velluti, F.; Mosconi, N.; Acevedo, A.; Borthagaray, G.; Castiglioni, J.; Faccio, R.; Back, D.F.; Moyna, G.; Rizzotto, M.; Torre, M.H. Synthesis, characterization, microbiological evaluation, genotoxicity and synergism tests of new nano silver complexes with sulfamoxole X-ray diffraction of $[Ag_2(SMX)_2]$·DMSO. *J. Inorg. Biochem.* **2014**, *141*, 58–69. [CrossRef] [PubMed]
8. Kohlmann, F.W.; Kuhne, J.; Wagener, H.H.; Weifenbach, H. Studies on microbiology and pharmacology of sulfaguanol, a new sulfonamide with effect on the intestines. *Arzneimittelforschung* **1973**, *23*, 172–178.
9. Kim, H.J.; Ryu, H.; Song, J.-Y.; Hwang, S.-G.; Jalde, S.S.; Choi, H.-K.; Ahn, J. Discovery of Oxazol-2-amine Derivatives as Potent Novel FLT3 Inhibitors. *Molecules* **2020**, *25*, 5154. [CrossRef] [PubMed]
10. Schmitt, F.; Gosch, L.C.; Dittmer, A.; Rothemund, M.; Mueller, T.; Schobert, R.; Biersack, B.; Volkamer, A.; Höpfner, M. Oxazole-Bridged Combretastatin A-4 Derivatives with Tethered Hydroxamic Acids: Structure–Activity Relations of New Inhibitors of HDAC and/or Tubulin Function. *Int. J. Mol. Sci.* **2019**, *20*, 383. [CrossRef] [PubMed]
11. Matio Kemkuignou, B.; Treiber, L.; Zeng, H.; Schrey, H.; Schobert, R.; Stadler, M. Macrooxazoles A–D, New 2,5-Disubstituted Oxazole-4-Carboxylic Acid Derivatives from the Plant Pathogenic Fungus *Phoma macrostoma*. *Molecules* **2020**, *25*, 5497. [CrossRef] [PubMed]
12. Jakeman, D.L.; Bandi, S.; Graham, C.L.; Reid, T.R.; Wentzell, J.R.; Douglas, S.E. Antimicrobial Activities of Jadomycin B and Structurally Related Analogues. *Antimicrob. Agents Chemother.* **2009**, *53*, 1245–1247. [CrossRef] [PubMed]
13. De Koning, C.B.; Ngwira, K.J.; Rousseau, A.L. Biosynthesis, synthetic studies, and biological activities of the jadomycin alkaloids and related analogues. In *The Alkaloids: Chemistry and Biology*; Knölker, H.-J., Ed.; Academic Press: Cambridge, MA, USA, 2020; Volume 84, pp. 125–199. ISBN 978-0-12-820982-0.
14. De Azeredo, C.M.O.; Ávila, E.P.; Pinheiro, D.L.J.; Amarante, G.W.; Soares, M.J. Biological activity of the azlactone derivative EPA-35 against *Trypanosoma cruzi*. *FEMS Microbiol. Lett.* **2017**, *364*, fnx020. [CrossRef]
15. Pinto, I.L.; West, A.; Debouck, C.M.; DiLella, A.G.; Gorniak, J.G.; O'Donnell, K.C.; O'Shannessy, D.J.; Patel, A.; Jarvest, R.L. Novel, selective mechanism-based inhibitors of the herpes proteases. *Bioorg. Med. Chem. Lett.* **1996**, *6*, 2467–2472. [CrossRef]
16. Bhandari, S.; Bisht, K.S.; Merkler, D.J. The Biosynthesis and Metabolism of the *N*-Acylated Aromatic Amino Acids: *N*-Acylphenylalanine, *N*-Acyltyrosine, *N*-Acyltryptophan, and *N*-Acylhistidine. *Front. Mol. Biosci.* **2022**, *8*, 801749. [CrossRef] [PubMed]
17. Arul Prakash, S.; Kamlekar, R.K. Function and therapeutic potential of *N*-acyl amino acids. *Chem. Phys. Lipids* **2021**, *239*, 105114. [CrossRef] [PubMed]
18. Battista, N.; Bari, M.; Bisogno, T. *N*-Acyl Amino Acids: Metabolism, Molecular Targets, and Role in Biological Processes. *Biomolecules* **2019**, *9*, 822. [CrossRef] [PubMed]
19. Burstein, S.H. *N*-Acyl Amino Acids (Elmiric Acids): Endogenous Signaling Molecules with Therapeutic Potential. *Mol. Pharmacol.* **2018**, *93*, 228–238. [CrossRef]
20. Wei, C.-W.; Yu, Y.-L.; Chen, Y.-H.; Hung, Y.-T.; Yiang, G.-T. Anticancer effects of methotrexate in combination with α-tocopherol and α-tocopherol succinate on triple-negative breast cancer. *Oncol. Rep.* **2019**, *41*, 2060–2066. [CrossRef]
21. Ezeriņa, D.; Takano, Y.; Hanaoka, K.; Urano, Y.; Dick, T.P. N-Acetyl Cysteine Functions as a Fast-Acting Antioxidant by Triggering Intracellular H_2S and Sulfane Sulfur Production. *Cell Chem. Biol.* **2018**, *25*, 447–459.e4. [CrossRef] [PubMed]
22. Chikukwa, M.T.R.; Walker, R.B.; Khamanga, S.M.M. Formulation and Characterisation of a Combination Captopril and Hydrochlorothiazide Microparticulate Dosage Form. *Pharmaceutics* **2020**, *12*, 712. [CrossRef] [PubMed]
23. Lockbaum, G.J.; Henes, M.; Lee, J.M.; Timm, J.; Nalivaika, E.A.; Thompson, P.R.; Kurt Yilmaz, N.; Schiffer, C.A. Pan-3C Protease Inhibitor Rupintrivir Binds SARS-CoV-2 Main Protease in a Unique Binding Mode. *Biochemistry* **2021**, *60*, 2925–2931. [CrossRef]
24. Vandyck, K.; Deval, J. Considerations for the discovery and development of 3-chymotrypsin-like cysteine protease inhibitors targeting SARS-CoV-2 infection. *Curr. Opin. Virol.* **2021**, *49*, 36–40. [CrossRef]

25. Van Dycke, J.; Dai, W.; Stylianidou, Z.; Li, J.; Cuvry, A.; Roux, E.; Li, B.; Rymenants, J.; Bervoets, L.; de Witte, P.; et al. A Novel Class of Norovirus Inhibitors Targeting the Viral Protease with Potent Antiviral Activity In Vitro and In Vivo. *Viruses* **2021**, *13*, 1852. [CrossRef] [PubMed]
26. Semple, G.; Ashworth, D.M.; Batt, A.R.; Baxter, A.J.; Benzies, D.W.M.; Elliot, L.H.; Evans, D.M.M.; Franklin, R.J.; Hudson, P.; Jenkins, P.D.; et al. Peptidomimetic aminomethylene ketone inhibitors of interleukin-1β-converting enzyme (ICE). *Bioorg. Med. Chem. Lett.* **1998**, *8*, 959–964. [CrossRef]
27. Deng, H.; Bannister, T.D.; Jin, L.; Babine, R.E.; Quinn, J.; Nagafuji, P.; Celatka, C.A.; Lin, J.; Lazarova, T.I.; Rynkiewicz, M.J.; et al. Synthesis, SAR exploration, and X-ray crystal structures of factor XIa inhibitors containing an α-ketothiazole arginine. *Bioorg. Med. Chem. Lett.* **2006**, *16*, 3049–3054. [CrossRef]
28. Allen, L.A.T.; Raclea, R.-C.; Natho, P.; Parsons, P.J. Recent advances in the synthesis of α-amino ketones. *Org. Biomol. Chem.* **2021**, *19*, 498–513. [CrossRef]
29. Rashdan, H.R.M.; Shehadi, I.A.; Abdelrahman, M.T.; Hemdan, B.A. Antibacterial Activities and Molecular Docking of Novel Sulfone Biscompound Containing Bioactive 1,2,3-Triazole Moiety. *Molecules* **2021**, *26*, 4817. [CrossRef]
30. Ahmad, I. Shagufta Sulfones: An Important Class of Organic Compounds with Diverse Biological Activities. *Int. J. Pharm. Pharm. Sci.* **2015**, *7*, 19–27.
31. Apostol, T.-V.; Drăghici, C.; Socea, L.-I.; Olaru, O.T.; Șaramet, G.; Enache-Preoteasa, C.; Bărbuceanu, Ș.-F. Synthesis, Characterization and Cytotoxicity Evaluation of New Diphenyl Sulfone Derivatives. *Farmacia* **2021**, *69*, 657–669. [CrossRef]
32. Mady, M.F.; Awad, G.E.A.; Jørgensen, K.B. Ultrasound-assisted synthesis of novel 1,2,3-triazoles coupled diaryl sulfone moieties by the CuAAC reaction, and biological evaluation of them as antioxidant and antimicrobial agents. *Eur. J. Med. Chem.* **2014**, *84*, 433–443. [CrossRef]
33. Guzmán-Ávila, R.; Avelar, M.; Márquez, E.A.; Rivera-Leyva, J.C.; Mora, J.R.; Flores-Morales, V.; Rivera-Islas, J. Synthesis, In Vitro, and In Silico Analysis of the Antioxidative Activity of Dapsone Imine Derivatives. *Molecules* **2021**, *26*, 5747. [CrossRef]
34. Fernández-Villa, D.; Aguilar, M.R.; Rojo, L. Folic Acid Antagonists: Antimicrobial and Immunomodulating Mechanisms and Applications. *Int. J. Mol. Sci.* **2019**, *20*, 4996. [CrossRef]
35. Kumar Verma, S.; Verma, R.; Xue, F.; Kumar Thakur, P.; Girish, Y.R.; Rakesh, K.P. Antibacterial activities of sulfonyl or sulfonamide containing heterocyclic derivatives and its structure-activity relationships (SAR) studies: A critical review. *Bioorg. Chem.* **2020**, *105*, 104400. [CrossRef] [PubMed]
36. Madduluri, V.K.; Baig, N.; Chander, S.; Murugesan, S.; Sah, A.K. Mo(VI) complex catalysed synthesis of sulfones and their modification for anti-HIV activities. *Catal. Commun.* **2020**, *137*, 105931. [CrossRef]
37. Xu, S.; Song, S.; Sun, L.; Gao, P.; Gao, S.; Ma, Y.; Kang, D.; Cheng, Y.; Zhang, X.; Cherukupalli, S.; et al. Indolylarylsulfones bearing phenylboronic acid and phenylboronate ester functionalities as potent HIV-1 non-nucleoside reverse transcriptase inhibitors. *Bioorg. Med. Chem.* **2022**, *53*, 116531. [CrossRef]
38. Regueiro-Ren, A. Cyclic sulfoxides and sulfones in drug design. In *Advances in Heterocyclic Chemistry*; Meanwell, N.A., Lolli, M.L., Eds.; Academic Press: Cambridge, MA, USA, 2021; Volume 134, pp. 1–30. ISBN 978-0-12-820181-7.
39. Feng, M.; Tang, B.; Liang, S.H.; Jiang, X. Sulfur Containing Scaffolds in Drugs: Synthesis and Application in Medicinal Chemistry. *Curr. Top. Med. Chem.* **2016**, *16*, 1200–1216. [CrossRef]
40. Kucwaj-Brysz, K.; Baltrukevich, H.; Czarnota, K.; Handzlik, J. Chemical update on the potential for serotonin 5-HT_6 and 5-HT_7 receptor agents in the treatment of Alzheimer's disease. *Bioorg. Med. Chem. Lett.* **2021**, *49*, 128275. [CrossRef] [PubMed]
41. Apostol, T.-V.; Draghici, C.; Dinu, M.; Barbuceanu, S.-F.; Socea, L.I.; Saramet, I. Synthesis, Characterization and Biological Evaluation of New 5-aryl-4-methyl-2-[*para*-(phenylsulfonyl)phenyl]oxazoles. *Rev. Chim.* **2011**, *62*, 142–148.
42. Apostol, T.-V.; Saramet, I.; Draghici, C.; Barbuceanu, S.-F.; Socea, L.I.; Almajan, G.L. Synthesis and Characterization of New 5-Aryl-2-[*para*-(4-chlorophenylsulfonyl)phenyl]-4-methyloxazoles. *Rev. Chim.* **2011**, *62*, 486–492.
43. Apostol, T.-V.; Barbuceanu, S.-F.; Olaru, O.T.; Draghici, C.; Saramet, G.; Socea, B.; Enache, C.; Socea, L.-I. Synthesis, Characterization and Cytotoxicity Evaluation of New Compounds from Oxazol-5(4*H*)-ones and Oxazoles Class Containing 4-(4-Bromophenylsulfonyl)phenyl Moiety. *Rev. Chim.* **2019**, *70*, 1099–1107. [CrossRef]
44. Apostol, T.V.; Barbuceanu, S.F.; Socea, L.I.; Draghici, C.; Saramet, G.; Iscrulescu, L.; Olaru, O.T. Synthesis, Characterization and Cytotoxicity Evaluation of New Heterocyclic Compounds with Oxazole Ring Containing 4-(Phenylsulfonyl)phenyl Moiety. *Rev. Chim.* **2019**, *70*, 3793–3801. [CrossRef]
45. Apostol, T.-V.; Socea, L.-I.; Drăghici, C.; Olaru, O.T.; Șaramet, G.; Enache-Preoteasa, C.; Bărbuceanu, Ș.-F. Design, Synthesis, Characterization, and Cytotoxicity Evaluation of New 4-Benzyl-1,3-oxazole Derivatives Bearing 4-(4-Chlorophenylsulfonyl)phenyl Moiety. *Farmacia* **2021**, *69*, 314–324. [CrossRef]
46. Apostol, T.V.; Drăghici, C.; Socea, L.I.; Olaru, O.T.; Șaramet, G.; Hrubaru, M.; Bărbuceanu, Ș.F. Synthesis, Characterization and Cytotoxicity Assessment of New 4-Benzyl-1,3-oxazole Derivatives Incorporating 4-[(4-Bromophenyl)sulfonyl]phenyl Fragment. *Farmacia* **2021**, *69*, 521–529. [CrossRef]
47. Guilhermino, L.; Diamantino, T.; Silva, M.C.; Soares, A.M.V.M. Acute Toxicity Test with *Daphnia magna*: An Alternative to Mammals in the Prescreening of Chemical Toxicity? *Ecotoxicol. Environ. Saf.* **2000**, *46*, 357–362. [CrossRef]
48. Seremet, O.C.; Olaru, O.T.; Gutu, C.M.; Nitulescu, G.M.; Ilie, M.; Negres, S.; Zbarcea, C.E.; Purdel, C.N.; Spandidos, D.A.; Tsatsakis, A.M.; et al. Toxicity of plant extracts containing pyrrolizidine alkaloids using alternative invertebrate models. *Mol. Med. Rep.* **2018**, *17*, 7757–7763. [CrossRef]

49. Lagunin, A.; Stepanchikova, A.; Filimonov, D.; Poroikov, V. PASS: Prediction of activity spectra for biologically active substances. *Bioinformatics* **2000**, *16*, 747–748. [CrossRef]
50. Mavrodin, A.; Oteleanu, D.; Vorel-Stoenescu, M.; Zotta, V. Studies on the sulfone group. IV. New sulfone-hydrazide derivatives. *Pharm. Zent. Dtschl.* **1956**, *95*, 353–361.
51. Schiketanz, I.; Draghici, C.; Saramet, I.; Balaban, A.T. Aminoketone, oxazole and thiazole synthesis. Part 15.[1] 2-[4-(4-Halobenzenesulphonyl)-phenyl]-5-aryloxazoles. *Arkivoc* **2002**, *2002*, 64–72. [CrossRef]
52. Cui, S.-Q.; Liao, W.-W. Recent Advances in Transition-Metal-Catalyzed C–H Addition to Nitriles. *Synthesis* **2022**, *54*, 33–48. [CrossRef]
53. da Rosa, R.; Grand, L.; Schenkel, E.P.; Campos Bernardes, L.S.; Jacolot, M.; Popowycz, F. The Use of 5-Hydroxymethylfurfural towards Fine Chemicals: Synthesis and Direct Arylation of 5-HMF-Based Oxazoles. *Synlett* **2021**, *32*, 838–844. [CrossRef]
54. Wei, L.; You, S.; Tuo, Y.; Cai, M. A Highly Efficient Heterogeneous Copper-Catalyzed Oxidative Cyclization of Benzylamines and 1,3-Dicarbonyl Compounds To Give Trisubstituted Oxazoles. *Synthesis* **2019**, *51*, 3091–3100. [CrossRef]
55. Murru, S.; Bista, R.; Nefzi, A. Synthesis of Novel Oxazolyl Amino Acids and Their Use in the Parallel Synthesis of Disubstituted Oxazole Libraries. *Synthesis* **2018**, *50*, 1546–1554. [CrossRef]
56. Katariya, K.D.; Vennapu, D.R.; Shah, S.R. Synthesis and molecular docking study of new 1,3-oxazole clubbed pyridyl-pyrazolines as anticancer and antimicrobial agents. *J. Mol. Struct.* **2021**, *1232*, 130036. [CrossRef]
57. Metelytsia, L.O.; Trush, M.M.; Kovalishyn, V.V.; Hodyna, D.M.; Kachaeva, M.V.; Brovarets, V.S.; Pilyo, S.G.; Sukhoveev, V.V.; Tsyhankov, S.A.; Blagodatnyi, V.M.; et al. 1,3-Oxazole derivatives of cytisine as potential inhibitors of glutathione reductase of *Candida spp.*: QSAR modeling, docking analysis and experimental study of new anti-Candida agents. *Comput. Biol. Chem.* **2021**, *90*, 107407. [CrossRef]
58. Ghazvini, M.; Sheikholeslami-Farahani, F.; Hamedani, N.F.; Shahvelayati, A.S.; Rostami, Z. Bio-Fe_3O_4 Magnetic Nanoparticles Promoted Green Synthesis of thioxo- 1,3-Oxazole Derivatives: Study of Antimicrobial and Antioxidant Activity. *Comb. Chem. High Throughput Screen.* **2021**, *24*, 1261–1270. [CrossRef] [PubMed]
59. Keivanloo, A.; Abbaspour, S.; Sepehri, S.; Bakherad, M. Synthesis, Antibacterial Activity and Molecular Docking Study of a Series of 1,3-Oxazole-Quinoxaline Amine Hybrids. *Polycycl. Aromat. Compd.* **2022**, *42*, 2378–2391. [CrossRef]
60. Ansari, A.; Ali, A.; Asif, M.; Rauf, M.A.; Owais, M. Shamsuzzaman Facile one-pot multicomponent synthesis and molecular docking studies of steroidal oxazole/thiazole derivatives with effective antimicrobial, antibiofilm and hemolytic properties. *Steroids* **2018**, *134*, 22–36. [CrossRef]
61. Wales, S.M.; Hammer, K.A.; Somphol, K.; Kemker, I.; Schröder, D.C.; Tague, A.J.; Brkic, Z.; King, A.M.; Lyras, D.; Riley, T.V.; et al. Synthesis and Antimicrobial Activity of Binaphthyl-Based, Functionalized Oxazole and Thiazole Peptidomimetics. *Org. Biomol. Chem.* **2015**, *13*, 10813–10824. [CrossRef]
62. Stokes, N.R.; Baker, N.; Bennett, J.M.; Chauhan, P.K.; Collins, I.; Davies, D.T.; Gavade, M.; Kumar, D.; Lancett, P.; Macdonald, R.; et al. Design, synthesis and structure–activity relationships of substituted oxazole–benzamide antibacterial inhibitors of FtsZ. *Bioorg. Med. Chem. Lett.* **2014**, *24*, 353–359. [CrossRef]
63. Marc, G.; Araniciu, C.; Oniga, S.D.; Vlase, L.; Pîrnău, A.; Duma, M.; Măruțescu, L.; Chifiriuc, M.C.; Oniga, O. New *N*-(oxazolylmethyl)-thiazolidinedione Active against *Candida albicans* Biofilm: Potential Als Proteins Inhibitors. *Molecules* **2018**, *23*, 2522. [CrossRef]
64. Juhás, M.; Bachtíková, A.; Nawrot, D.E.; Hatoková, P.; Pallabothula, V.S.K.; Diepoltová, A.; Jand'ourek, O.; Bárta, P.; Konečná, K.; Paterová, P.; et al. Improving Antimicrobial Activity and Physico-Chemical Properties by Isosteric Replacement of 2-Aminothiazole with 2-Aminooxazole. *Pharmaceuticals* **2022**, *15*, 580. [CrossRef]
65. Apostol, T.-V.; Chifiriuc, M.C.; Nitulescu, G.M.; Olaru, O.T.; Barbuceanu, S.-F.; Socea, L.-I.; Pahontu, E.M.; Karmezan, C.M.; Marutescu, L.G. In Silico and In Vitro Assessment of Antimicrobial and Antibiofilm Activity of Some 1,3-Oxazole-Based Compounds and Their Isosteric Analogues. *Appl. Sci.* **2022**, *12*, 5571. [CrossRef]
66. Molchanova, N.; Nielsen, J.E.; Sørensen, K.B.; Prabhala, B.K.; Hansen, P.R.; Lund, R.; Barron, A.E.; Jenssen, H. Halogenation as a tool to tune antimicrobial activity of peptoids. *Sci. Rep.* **2020**, *10*, 14805. [CrossRef]
67. Cruz, J.C.S.; Iorio, M.; Monciardini, P.; Simone, M.; Brunati, C.; Gaspari, E.; Maffioli, S.I.; Wellington, E.; Sosio, M.; Donadio, S. Brominated Variant of the Lantibiotic NAI-107 with Enhanced Antibacterial Potency. *J. Nat. Prod.* **2015**, *78*, 2642–2647. [CrossRef]
68. Gottardi, W.; Klotz, S.; Nagl, M. Superior bactericidal activity of *N*-bromine compounds compared to their *N*-chlorine analogues can be reversed under protein load. *J. Appl. Microbiol.* **2014**, *116*, 1427–1437. [CrossRef]
69. Barbuceanu, S.-F.; Almajan, G.L.; Saramet, I.; Draghici, C.; Tarcomnicu, A.I.; Bancescu, G. Synthesis, characterization and evaluation of antibacterial activity of some thiazolo[3,2-b][1,2,4]triazole incorporating diphenylsulfone moieties. *Eur. J. Med. Chem.* **2009**, *44*, 4752–4757. [CrossRef]
70. Apostol, T.-V.; Marutescu, L.G.; Draghici, C.; Socea, L.-I.; Olaru, O.T.; Nitulescu, G.M.; Pahontu, E.M.; Saramet, G.; Enache-Preoteasa, C.; Barbuceanu, S.-F. Synthesis and Biological Evaluation of New *N*-Acyl-α-amino Ketones and 1,3-Oxazoles Derivatives. *Molecules* **2021**, *26*, 5019. [CrossRef]
71. Apostol, T.-V.; Chifiriuc, M.C.; Draghici, C.; Socea, L.-I.; Marutescu, L.G.; Olaru, O.T.; Nitulescu, G.M.; Pahontu, E.M.; Saramet, G.; Barbuceanu, S.-F. Synthesis, In Silico and In Vitro Evaluation of Antimicrobial and Toxicity Features of New 4-[(4-Chlorophenyl)sulfonyl]benzoic Acid Derivatives. *Molecules* **2021**, *26*, 5107. [CrossRef]

72. Zhang, W.; Liu, W.; Jiang, X.; Jiang, F.; Zhuang, H.; Fu, L. Design, synthesis and antimicrobial activity of chiral 2-(substituted-hydroxyl)-3-(benzo[d]oxazol-5-yl)propanoic acid derivatives. *Eur. J. Med. Chem.* **2011**, *46*, 3639–3650. [CrossRef] [PubMed]
73. Desai, N.C.; Vaja, D.V.; Joshi, S.B.; Khedkar, V.M. Synthesis and molecular docking study of pyrazole clubbed oxazole as antibacterial agents. *Res. Chem. Intermed.* **2021**, *47*, 573–587. [CrossRef]
74. Thatha, S.; Ummadi, N.; Venkatapuram, P.; Adivireddy, P. Synthesis, Characterization, and Antioxidant Activity of a New Class of Amido linked Azolyl Thiophenes. *J. Heterocycl. Chem.* **2018**, *55*, 1410–1418. [CrossRef]
75. Basha, N.M.; Reddy, P.R.; Padmaja, A.; Padmavathi, V. Synthesis and Antioxidant Activity of Bis-oxazolyl/thiazolyl/imidazolyl 1,3,4-Oxadiazoles and 1,3,4-Thiadiazoles. *J. Heterocycl. Chem.* **2016**, *53*, 1276–1283. [CrossRef]
76. Stankova, I.; Spasova, M. Hydroxycinnamic Acid Amides with Oxazole-Containing Amino Acid: Synthesis and Antioxidant Activity. *Z. Naturforsch. C* **2009**, *64*, 176–178. [CrossRef]
77. Kumar, G.; Singh, N.P. Synthesis, anti-inflammatory and analgesic evaluation of thiazole/oxazole substituted benzothiazole derivatives. *Bioorg. Chem.* **2021**, *107*, 104608. [CrossRef]
78. Mendez, D.; Gaulton, A.; Bento, A.P.; Chambers, J.; De Veij, M.; Félix, E.; Magariños, M.P.; Mosquera, J.F.; Mutowo, P.; Nowotka, M.; et al. ChEMBL: Towards direct deposition of bioassay data. *Nucleic Acids Res.* **2019**, *47*, D930–D940. [CrossRef]
79. Sander, T.; Freyss, J.; von Korff, M.; Rufener, C. DataWarrior: An Open-Source Program For Chemistry Aware Data Visualization And Analysis. *J. Chem. Inf. Model.* **2015**, *55*, 460–473. [CrossRef]
80. Stepanović, S.; Vuković, D.; Hola, V.; Di Bonaventura, G.; Djukić, S.; Ćirković, I.; Ruzicka, F. Quantification of biofilm in microtiter plates: Overview of testing conditions and practical recommendations for assessment of biofilm production by staphylococci. *APMIS* **2007**, *115*, 891–899. [CrossRef] [PubMed]
81. Limban, C.; Balotescu Chifiriuc, M.-C.; Missir, A.-V.; Chiriţă, I.C.; Bleotu, C. Antimicrobial Activity of Some New Thioureides Derived from 2-(4-Chlorophenoxymethyl)benzoic Acid. *Molecules* **2008**, *13*, 567–580. [CrossRef]
82. Patrinoiu, G.; Calderón-Moreno, J.M.; Chifiriuc, C.M.; Saviuc, C.; Birjega, R.; Carp, O. Tunable ZnO spheres with high anti-biofilm and antibacterial activity *via* a simple green hydrothermal route. *J. Colloid Interface Sci.* **2016**, *462*, 64–74. [CrossRef] [PubMed]
83. Prodan, A.M.; Iconaru, S.L.; Chifiriuc, C.M.; Bleotu, C.; Ciobanu, C.S.; Motelica-Heino, M.; Sizaret, S.; Predoi, D. Magnetic Properties and Biological Activity Evaluation of Iron Oxide Nanoparticles. *J. Nanomater.* **2013**, *2013*, 893970. [CrossRef]
84. Munteanu, I.G.; Apetrei, C. Analytical Methods Used in Determining Antioxidant Activity: A Review. *Int. J. Mol. Sci.* **2021**, *22*, 3380. [CrossRef]
85. Ilyasov, I.R.; Beloborodov, V.L.; Selivanova, I.A.; Terekhov, R.P. ABTS/PP Decolorization Assay of Antioxidant Capacity Reaction Pathways. *Int. J. Mol. Sci.* **2020**, *21*, 1131. [CrossRef]
86. Mendonça, J.D.S.; de Cássia Avellaneda Guimarães, R.; Zorgetto-Pinheiro, V.A.; Fernandes, C.D.P.; Marcelino, G.; Bogo, D.; de Cássia Freitas, K.; Hiane, P.A.; de Pádua Melo, E.S.; Vilela, M.L.B.; et al. Natural Antioxidant Evaluation: A Review of Detection Methods. *Molecules* **2022**, *27*, 3563. [CrossRef]
87. Blois, M.S. Antioxidant Determinations by the Use of a Stable Free Radical. *Nature* **1958**, *181*, 1199–1200. [CrossRef]
88. Barbuceanu, S.-F.; Ilies, D.C.; Saramet, G.; Uivarosi, V.; Draghici, C.; Radulescu, V. Synthesis and Antioxidant Activity Evaluation of New Compounds from Hydrazinecarbothioamide and 1,2,4-Triazole Class Containing Diarylsulfone and 2,4-Difluorophenyl Moieties. *Int. J. Mol. Sci.* **2014**, *15*, 10908–10925. [CrossRef]
89. Ilies, D.-C.; Shova, S.; Radulescu, V.; Pahontu, E.; Rosu, T. Synthesis, characterization, crystal structure and antioxidant activity of Ni(II) and Cu(II) complexes with 2-formilpyridine *N*(4)-phenylthiosemicarbazone. *Polyhedron* **2015**, *97*, 157–166. [CrossRef]
90. Duan, X.-J.; Zhang, W.-W.; Li, X.-M.; Wang, B.-G. Evaluation of antioxidant property of extract and fractions obtained from a red alga, *Polysiphonia urceolata*. *Food Chem.* **2006**, *95*, 37–43. [CrossRef]
91. Re, R.; Pellegrini, N.; Proteggente, A.; Pannala, A.; Yang, M.; Rice-Evans, C. Antioxidant activity applying an improved ABTS radical cation decolorization assay. *Free Radic. Biol. Med.* **1999**, *26*, 1231–1237. [CrossRef]
92. Oyaizu, M. Studies on Products of Browning Reaction. Antioxidative Activities of Products of Browning Reaction Prepared from Glucosamine. *Japanese J. Nutr. Diet.* **1986**, *44*, 307–315. [CrossRef]
93. Dorman, H.J.D.; Koşar, M.; Kahlos, K.; Holm, Y.; Hiltunen, R. Antioxidant Properties and Composition of Aqueous Extracts from *Mentha* Species, Hybrids, Varieties, and Cultivars. *J. Agric. Food Chem.* **2003**, *51*, 4563–4569. [CrossRef]
94. Işıl Berker, K.; Güçlü, K.; Tor, I.; Apak, R. Comparative evaluation of Fe (III) reducing power-based antioxidant capacity assays in the presence of phenanthroline, *batho*-phenanthroline, tripyridyltriazine (FRAP), and ferricyanide reagents. *Talanta* **2007**, *72*, 1157–1165. [CrossRef] [PubMed]
95. OECD. *Test No. 202: Daphnia sp. Acute Immobilisation Test*; OECD Guidelines for the Testing of Chemicals, Section 2; OECD Publishing: Paris, France, 2004 ISBN 9789264069947.
96. Stecoza, C.E.; Nitulescu, G.M.; Draghici, C.; Caproiu, M.T.; Olaru, O.T.; Bostan, M.; Mihaila, M. Synthesis and Anticancer Evaluation of New 1,3,4-Oxadiazole Derivatives. *Pharmaceuticals* **2021**, *14*, 438. [CrossRef] [PubMed]
97. Nitulescu, G.; Mihai, D.P.; Nicorescu, I.M.; Olaru, O.T.; Ungurianu, A.; Zanfirescu, A.; Nitulescu, G.M.; Margina, D. Discovery of natural naphthoquinones as sortase A inhibitors and potential anti-infective solutions against *Staphylococcus aureus*. *Drug Dev. Res.* **2019**, *80*, 1136–1145. [CrossRef] [PubMed]
98. Zakharov, A.V.; Peach, M.L.; Sitzmann, M.; Nicklaus, M.C. A New Approach to Radial Basis Function Approximation and Its Application to QSAR. *J. Chem. Inf. Model.* **2014**, *54*, 713–719. [CrossRef]